Ultra Low-Loss and Wideband Photonic Crystal Waveguides for Dense Photonic Integrated Systems

A Thesis

Presented to

The Academic Faculty

by

Aliakbar Jafarpour

In Partial Fulfillment
of the Requirements for the Degree
Doctor of Philosophy in Electrical and Computer Engineering

School of Electrical and Computer Engineering

Georgia Institute of Technology

August 2006

Ultra Low-Loss and Wideband Photonic Crystal Waveguides for Dense Photonic Integrated Systems

Approved by:

Dr. Ali Adibi
School of ECE
Georgia Institute of Technology

Dr. Rick Trebino
School of Phys
Georgia Institute of Technology

Dr. Thomas K. Gaylord
School of ECE
Georgia Institute of Technology

Dr. W. Russell Callen Jr.
School of ECE
Georgia Institute of Technology

Dr. Russell Dean Dupuis
School of ECE
Georgia Institute of Technology

Dr. Joseph Perry
School of Chem
Georgia Institute of Technology

Date approved: July 10, 2006

ACKNOWLEDGEMENTS

I would like to express my deep appreciation to my thesis advisor, Prof. Ali Adibi for all his support, encouragement, and research directions. I would also like to thank my co-advisor, Prof. Rick Trebino; the Thesis Committee members, Professors Thomas K. Gaylord, Russell Callen Jr., Russell Dean Dupuis, and Joseph Perry; and also my former advisor, Professor Mohammad Etrati Khosrohahi for their guidance.

I would like to thank Dr. Sina Khorasani, Mohammad, and Babak for their helps and most importantly their visions and commitment to principles and research ethics.

I am grateful to Professor Yong Xu (Virginia Polytechnic Institute), Dr. Edmond Chow (Agilent Technologies), Mr. Gary Eisenmann (Coherent Inc.), trainers of the Microelectronics Research Center (Georgia Tech), and members of FROG group, especially Aparna, Selcuk, Xun, Mark, and Pablo for their technical helps.

I had the pleasure of having useful discussions with and receiving technical helps from JD, Siva, Murtaza, Ehsan, Pejman, Reza, and Amir Hossein. I am grateful to Omid and Arash for their helps and being there for me, when needed. I had the pleasure of having nice colleagues like Cheryl, Henry, Saeed, Majid, Jerry, Charlie, Charles, Fengtao, Ye, Pouyan, Ali, Nancy, and Angela; thank you all for your helps and supports.

Finally, my wordless gratitude goes to my beloved family, especially my dear parents, for all their love and support.

TABLE OF CONTENTS

LIST OF FIGURES

SUMMARY

This thesis reports on a new design of photonic crystal waveguides (PCWs) to achieve large guiding bandwidth, linear dispersion, single-mode behavior, good coupling efficiency to dielectric waveguides, and small loss. The design is based on using the linear dispersion region of one PCW in the photonic bandgap (PBG) of another PCW. While perturbing the period can result in a PCW with linear dispersion and large guiding bandwidth, it introduces an odd mode at those frequencies, as well. By using another perturbation scheme, it is shown that single-mode behavior can also be achieved. The linear dispersion of these waveguides and their operation at lower frequencies of the PBG, where the density of states of radiation modes is smaller, gives rise to very small loss coefficients as verified experimentally.

Full characterization of a waveguide requires the measurement of not only the transmission coefficient, but also the dispersion and spectral phase. We have developed a real-time characterization technique based on spectral interferometry with femtosecond laser pulses at optical communication wavelengths to measure the spectral phase of waveguides. This characterization technique can be used to study fast dynamics in time-varying structures and makes the alignment easy.

CHAPTER I

AN INTRODUCTION TO PHOTONIC CRYSTALS

1.1. Why Photonic Crystal Waveguides?

The short history of photonic crystals dates back to 1987, when two papers were published in an edition of Physical Review Letters [1,2] and reported the idea of *Photonic Band Gap* (PBG). Although wave propagation in periodic media (including gratings and even 2D optical lattices) had been known for a long time, these studies created a new direction of theoretical and experimental research. The main concern of the 1987 papers was to engineer the density of (optical) states in some synthetic materials and to eliminate spontaneous emission of light; thereby improving the performance of lasers. It was shown that the propagation of optical waves in a medium with a periodic index of refraction parallels the propagation of electronic wave functions (i.e., motion of electrons) in semiconductors and electronic lattices. This analogy led to the term *photonic crystals* (PCs) as opposed to *electronic crystals*.

Some researchers focused on the original theme of the story and studied quantum electrodynamics [3] and density of (optical) states [4] in PCs in detail. However, the majority of research concentrated on:

a) Optical counterparts of various concepts in solid-state physics and electronic crystals (band diagrams [5], guided modes [6], bound states [7], …)

b) Novel optical phenomena that had not been observed in conventional optical

materials (superprism [8], negative refraction, negative diffraction, optically-induced shock waves [9]…)

c) PC-based optical functionalities (demultiplexers, waveguides, oscillators, filters, couplers, ….) using the results of the previous two categories [10]

Successful application of microelectronics fabrication technology in realization of PCs and promising characterization results of individual PC-based devices led to the idea of PCs as suitable platforms for *photonic integrated systems* (optical ICs) and also optical-electrical chips. However, there were some challenges in realization of such PC-based systems. Some of the most important challenges were different issues associated with photonic crystal waveguides (PCWs). While PCWs can guide optical beams under certain conditions, they cannot meet the needs of photonic integrated systems. The goal of this thesis is to get a deeper insight into the nature of wave propagation in PCWs; to propose and demonstrate ideas that improve the performance of PCWs; and to introduce a novel characterization technique for real-time full characterization of PCWs.

1.2. Fundamental Concepts

Photonic crystals (PCs) can be made by introducing a 1-dimensional (1D), 2-dimenstional (2D), or a 3-dimensional (3D) periodicity in the index of refraction of a structure. PCs are inhomogeneous materials and plane waves are not eigenfunctions of the Helmholtz equation in such structures. The total field in a PC is the sum of the incident field and the fields reflected off all scattering regions (distributed Bragg reflection or DBR). Depending on the period of the structure and the frequency of operation, DBR and the incident field can add constructively or destructively. A

resonance condition occurs when backward-propagating waves completely cancel out forward-propagating waves and the transmission coefficient vanishes. Thus, PCs can have some gaps (referred to as photonic bandgaps or PBGs [1,2,5]) in their band diagrams; i.e., in the diagram of energy versus momentum of photons. In other words, electromagnetic waves with certain frequencies cannot propagate in these structures.

1.3. Analogy with Electronic Crystals

Electronic wave functions propagate in electronic crystals according to a second order partial differential equation (Schrödinger's wave equation). Bragg reflections of the scalar wave function in the presence of a periodic electric potential will result in spatial wave packets in the form of Floquet components (diffracted orders), mode coupling and folding, and also *electronic* bandgaps in the band diagram (energy versus momentum of *electrons*). Introducing a defect in an otherwise-uniform crystal will result in new localized or guided modes in the bandgap of the unperturbed lattice.

In the same way, *electromagnetic waves* propagate in photonic crystals according to a second order partial differential equation (Helmholtz equation). Bragg reflections of the vectorial electromagnetic fields in the presence of a periodic dielectric constant will result in spatial wave packets in the form of Floquet components (diffracted orders), mode coupling and folding, and also *photonic* bandgaps in the band diagram (energy versus momentum of *photons*). Introducing a defect in an otherwise-uniform crystal will result in new localized or guided modes in the bandgap of the unperturbed lattice.

Note that the existence of a PBG in a PC and consequent properties are classical electromagnetic effects. However, it is sometimes easier to use the quantum

electrodynamic (QED) picture of light in describing this classical phenomenon. The band diagram, for instance, can be interpreted as the graph of energy vs. momentum of photons.

1.4. Geometries

PCs are divided into the following categories based on the complexities of their periodicities:

1.4.1. 3D PCs

a) They can have full (3D) PBGs for all possible directions of wave propagation.

b) A full 3D vectorial formulation of Maxwell's equations is needed to analyze these structures.

c) Numerical analysis of such structures requires considerable time and computational capacity. 3D numerical studies are limited to unit cells or relatively short structures.

1.4.2. 2D PCs

a) They can have PBGs for all directions of propagation in the plane of periodicity (2D PBG).

b) The plane of periodicity is uniformly and infinitely extended in the normal direction. It is impossible to realize an ideal 2D PC.

c) There are two decoupled sets of waves corresponding to two decoupled polarizations in these structures for in-plane wave propagation, unless the

substrates are anisotropic.

d) The TE (TM) polarization is defined here to have the electric (magnetic) field parallel to the axis of air holes.

e) It has been shown that a PC with a square (triangular) lattice can have a PBG for the TE (TM) polarization [11].

f) Electromagnetic equations describing (in-plane) wave propagation in such structures can be reduced to a scalar equation in terms of only one field component (E_z or H_z).

g) Cavities with very small mode volumes [12], very small bends with large transmission efficiencies [13], and nonlinear structures with controllable dispersion and phase matching [14] are some of the interesting applications of PCs.

h) Numerical simulation of such structures with relatively large sizes in a reasonable time is possible even with an ordinary personal computer.

1.4.3. 1D PCs (Gratings)

a) They can have PBGs for propagation along the direction of periodicity (1D PBG).

b) They are easier to simulate and can even have analytical solutions.

c) Exciting the structure in a unique direction of propagation can be a practical challenge.

There is also a fourth category referred to as photonic crystal slabs. A PC slab has a 2D periodicity, but is not uniform in the third direction. Almost all practical PCs are realized in the form of PC slabs. They are introduced in detail in section 1.6.

1.5. Simulation Techniques

Simulation methods such as the Plane Wave Method (PWM) [5], Scattering (or Transfer) Matrix [15], Green's Function [4], Finite Difference Time Domain (FDTD) [16], and also Finite Element Method (FEM) [17] have been widely used in the study of PC structures with their own advantages and limitations. The numerical techniques can be contrasted in different ways:

a) They may discretize space into different *grid points* (FDTD) or *meshes* (FEM). Having a Cartesian grid cell (as in FDTD) will result in problems in modeling triangular lattices. Having a good accuracy without increasing the simulation time requires different spatial resolutions in different parts of the domain of simulation. This requirement can be easily met by some methods (FEM), whereas it requires considerable modification of original formulations in FDTD.

b) The sampling may be done in real space (FDTD) or in the wavevector space (PWM). The accuracy of the methods will depend on the number of grid points per unit cell and the number of Floquet components, respectively.

c) They may implement Maxwell's equations directly (FDTD) or may propose a parametric solution of the fields and solve the problem partially before calculations (as in the PWM).

d) They may solve the equation in the time domain (FDTD) or in the frequency domain (PWM) by scanning the frequency axis over a bandwidth and assuming sinusoidal steady state in the structure (for any frequency), thereby eliminating one degree of freedom (time) in Maxwell's equations. One advantage of a time

domain technique is in using only one simulation to characterize a structure usually over a large bandwidth. The other advantage is having a high spectral resolution and capability of identifying resonances with high quality factors. A third advantage is the ability to model the transient response of a given structure. The disadvantage of a time domain technique is the inherent difficulty in characterizing a quasi-stationary state (needing an infinite simulation time).

e) They may be general (FDTD) or may rely on some limiting assumptions regarding the structure such as uniformity or periodicity (PWM).

f) Some methods may rely on simple equations and may need relatively small amount of computer memory (FDTD). On the other hand, some other methods may need to solve eigenvalue problems (PWM) or calculate inverse matrices and transcendental functions (Green's Function).

g) They may treat different regions (formed by different electrical properties) differently by using different field expansions (Green's Function), or they may essentially use the same formulation for all points (FDTD).

Unless otherwise stated, the simulation results reported here have been obtained using a 2D FDTD code.

1.6. Photonic Crystal Slabs

1.6.1. Basic Properties

A realistic and easy-to-fabricate PC structure is a truncated 2D PC, referred to as a *photonic crystal slab*. This geometry is compatible with planar microfabrication technology and is used in practical PCs. The highly-developed fabrication technology of

CMOS can be used to create PCs on silicon substrates and even combine them with electronic components [18]. The thickness of the structure in a PC slab is finite, and wavevectors are not necessarily in the plane of periodicity [19,20]. The PC pattern is usually a periodic pattern of cylindrical air holes etched into a dielectric slab.

1.6.2. Guided and Leaky Modes

The modes confined in a slab waveguide can only have wavevectors giving rise to total internal reflection by cladding regions. So, not all solutions to Maxwell's equations in a PC slab represent confined modes. A line described by $\omega=c/\beta$ and referred to as the *light line* separates the region of *guided* (below the light line) and *leaky* (above the light line) modes in the band diagram of PC slabs. A guided mode will propagate in the plane of a PC over any arbitrary distance with the same (Bloch) amplitude, and power is conserved in this propagation. A leaky mode, on the other hand, will leak electromagnetic power into the cladding regions during propagation.

Leaky modes, present above the light line in the band diagram of PC slabs, are represented by a decaying sinusoidal (other than the periodic Bloch function) in real space. They are also represented by decaying functions in time and a resonance with a linewidth in frequency space. For this reason, leaky modes are also called *guided resonances*. It has been verified experimentally and theoretically that guided resonances of PC slabs can have very high quality factors (greater than 3000) and propagate over lengths as large as 50 periods of the PC without appreciable change in their amplitude [21]. Longer PCs, however, have low or zero transmission coefficients for leaky modes at

frequencies above the light line. Hence, an easy way to determine the regions with leaky modes is to compare transmission spectra of short and long PC slab structures.

In practice, PC slabs also have some attenuation at frequencies with guided modes (below the light line). This attenuation is primarily the result of fabrication imperfections and unwanted scatterings and not an inherent property of the mode. It is not related to the extinction coefficient of the material, either. This attenuation is also modeled by a phenomenological loss coefficient, which is usually smaller than the loss coefficient of leaky modes for a good fabrication.

1.6.3. Energy Leakage and Density of States

The continuum of radiation modes above the light line has different Densities of States (DOS) at different frequencies. The DOS varies in proportion to the square of frequency in vacuum. As a result, a leaky mode will leak energy much more easily at higher frequencies, because of the high DOS of radiation modes. So, operation below and far from the light line at low frequencies is an important performance index of PCs, which will be considered in our optimization in the next chapters.

1.6.4. Two Separate Classes of Guided Modes

A PC slab supports two different sets of modes with even and odd symmetries with respect to the middle of the slab. These two sets correspond to the two TE and TM polarizations in the 2D case and are called TE-like and TM-like, respectively. (Note that TE and TM have been defined here with respect to the slab. A TE-like mode of a PC slab

has a magnetic field normal to the plane of periodicity and is the analogue of a TM mode in the 2D case).

PC slabs do not have PBGs like their 2D counterparts. There are some radiation modes above the light line at all frequencies. However, modes with the same transverse symmetry (TE-like or TM-like) can have *gaps of guided modes*; i.e., a frequency range with no guided modes (but with a continuum of radiation modes at each frequency).

1.6.5. Asymmetric PC Slabs

So far, we have concentrated on symmetric PC slabs that are somehow suspended in air. Practical PC slabs have usually an underlying dielectric layer for mechanical support, insulation, and partial protection against environmental damages. For PCs fabricated in Silicon on Insulators (SOIs), for instance, the PC pattern is defined on a silicon layer, and there is a thick silicon dioxide layer underneath the silicon layer. There is also another thick layer of silicon underneath the silicon dioxide layer. If the underlying oxide layer is removed, the geometry will still be asymmetric. However, the structure will be symmetric in the transverse direction within a few wavelengths from the slab, and the suspended structure will be (optically) symmetric. But what if the underlying material is not etched and the structure remains asymmetric?

Even in the 2D case, there are fundamental differences between symmetric and asymmetric slab waveguides. For example, the fundamental mode of an asymmetric slab waveguide can have a cutoff frequency. There will be more penetration of the guided waves into the higher-index cladding region, and the modes are not even and odd. Such differences will affect the properties of a PC fabricated on an asymmetric slab. The

guided modes cannot be classified according to their transverse symmetries. The guided modes will have no bandgap and the PC properties are apparently lost. However, if the mode is sufficiently localized in the slab, the high-index cladding will only be a small perturbation, and *some effects of the bandgap will persist* [19].

As a final note, the properties of all modes including those above the light line ("leaky modes") depend on the symmetry of the slab. Breaking this symmetry can result in no coupling between certain internal eigenmodes and external radiation modes. So, a mode above the light line is not necessarily leaky [21].

1.6.6. The Effective Index Method

A PC slab has a 2D periodicity (like a 2D PC), but requires a full vectorial 3D analysis (like a 3D PC), for the slab is not uniform in the transverse direction. The 3D simulation time of a 3D structure can be typically up to two orders of magnitude longer than that of the 2D counterpart. It also requires larger memory sizes. A solution to this problem is to use a 2D analysis, which also takes the third dimension into account. We use the effective index method to treat the PC slab as a 2D structure and study in-plane and transverse wave propagations separately. The refractive index of the substrate is replaced with an effective index, which is the guide index of the slab without any in-plane perturbations: $N_{eff}=\beta_{slab}/k_0$, where N_{eff} is the effective (in-plane) index of refraction; β_{slab} is the propagation constant of the slab (at the frequency of operation); and k_0 is the free space propagation constant (at the same frequency).

A 2D analysis of PC slabs is not an approximation to a 3D analysis. It also provides us with more insight into the nature of wave propagation. Many properties of PC slabs

can be qualitatively categorized as:

a) Those originating from the two dimensional (2D) periodicity, and

b) Those brought about by the coupling between in-plane and out-of-plane evolution of the field.

In analyzing a PC slab, it is still important to have some 2D analyses to identify the properties in the first category. One can then run a 3D simulation and the differences between the results of the two analyses are attributed to the second category.

The solutions obtained using the effective index method are more accurate compared to those obtained by just a 2D analysis. However, the effective index method, even if applied to uniform structures (like channel waveguides), has some errors (at low frequencies) [22]. Therefore it is reasonable to see some frequency shift of the spectral features obtained using the effective index method compared to the 3D results. This error can be minimized using schemes such as:

a) Correcting the inherent error of the effective index method [22].

b) One 3D and multiple 2D (with effective index) simulations of a *unit-cell* (that can be done quickly) to optimize the effective index used. The so-obtained effective index can then be used in 2D analyses of PCs with *arbitrary lengths and defects*.

Depending on the frequency of operation, the effective index can change. The accurate value can be obtained using a 3D simulation and some 2D simulations as mentioned above. It is noted that a 2D frequency-domain technique has no problem in handling a frequency-dependent effective refractive index. A time-domain technique can also implement such frequency dependence. However, it requires convolution of the electric field and the inverse Fourier transform of the dielectric function to calculate the

displacement vector in any time step. It will result in a more complicated formulation of Maxwell's equations and longer simulation times. If *inherent 2D properties* are concerned, the variations in the effective index can be neglected. Unless otherwise stated, the value of the effective refractive index used in our 2D simulations, is 7.9 [23].

1.6.7. Fabrication

Scalability of Maxwell's equations suggests that a linear electromagnetic system will have the same characteristics (except for a scale factor) if the geometry is scaled. For example, the electromagnetic response of an airplane to incident radar waves will be equivalent to those of a small model airplane, if tested with smaller wavelengths in a small lab. Using this property, early (and some of current) experiments on PCs have been done in the microwave (rather than optical) frequencies of the electromagnetic spectrum. As a result, the feature sizes – which are a few times smaller than the free-space wavelength of operation - have been relatively large and fabrications have been easy.

The most popular and applied wavelengths are optical communication wavelengths; around 1.3 and 1.55 microns or roughly speaking between 1-2 microns. It means feature sizes will be sub-micron or even sub-100nm. PCs are very sensitive to fabrication imperfections and if a lithography system works on the limit of its resolution, it will introduce considerable irregularities and unwanted optical scatterings. So, photolithography (even with a high resolution mask and vacuum-contact exposure) is not a good choice. A better solution is UV lithography, but there exists the same problem, here; having feature sizes comparable to the resolution of the system.

Electron beam lithography (EBL) is the most common choice for definition of PC

patterns. It is a *direct-write* technique and does not require a mask. EBL systems are commercially available from different vendors at different prices from $30K (as an SEM accessory) to $5M with different accuracies from sub-100nm to sub-10nm resolutions. Current electron-beam resists (such as ZEP-520A and PMMA) and developers (such as ZED-N50) have well-known characteristics and repeatable results. Also, the controllability of electron dose level provides users with flexibility in compensation for electron scattering and defining patterns with different sizes and different concentrations.

A good fabrication also involves a high-quality anisotropic etching of patterns after writing them on a sample and developing the sample. Anisotropic plasma etching with optimized concentrations of gases such as Ar, O_2, H_2, He, BCl_3, SF_6, Cl_2, CF_4, CHF_3, and HBr (in different etch chemistries) is used to transfer the PC patterns to the slab. A final wet etching is needed, if a symmetric suspended slab is required [24].

There is also a possibility for using e*merging nanolithography systems*. A Focused Ion Beam (FIB) system, for instance, uses a principle similar to EBL, but with heavy and high-energy ions of gallium rather than electrons. There have been reports of fabricating PC slabs using FIB (combined with optical lithography) [25]. However, FIB is still in the research phase and FIB fabrication processes have not been developed like those of EBL.

1.6.8. Regimes of Operation

A PC slab can be used in two different regimes of operation:

a) At frequencies out of the PBG to use specific properties of the PC such as superprism, negative diffraction, and negative refraction.

b) At frequencies within the PBG to simply act as a “mirror”. Introducing defects in

an otherwise-periodic PC will result in guided or localized modes, for photons are reflected off the PC mirrors.

In both above-mentioned cases, electromagnetic waves propagate in the plane of periodicity. However, it is also possible to have a "PC", in which the direction of propagation is normal to the plane of periodicity. A practical example is a photonic crystal fiber, in which the cladding region has a periodic transverse pattern.

We are not concerned with PC fibers or planar PCs operating at frequencies out of the PBG. The main focus here is on waveguides operating at PBG frequencies.

1.7. Concluding Remarks

In summary, we have reviewed the main properties of PC slabs. PCWs and the problems associated with them will be introduced in Chapter 2. Unless otherwise stated, the simulations reported here have been done by a 2D FDTD code with an effective dielectric constant of 7.9 and a radius to pitch ratio of r/a=0.3 to have a large PBG for TM polarization (magnetic field normal to the plane of periodicity). The band diagram of such a PC (shown in Figure 1.1(a)) for TM polarization has been shown in Figure 1.1(b). It is clearly seen that the structure has a PBG in the frequency range of 0.253 to 0.32.

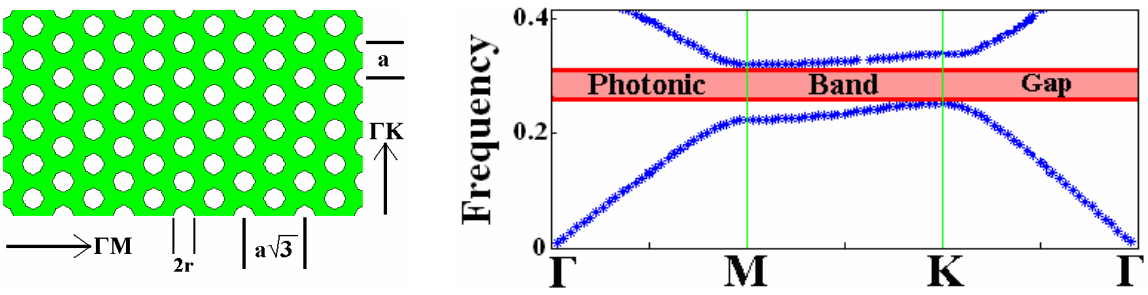

(a) (b)

Figure 1.1. (a) A triangular lattice photonic crystal and (b) the associated band diagram.

CHAPTER II

PHOTONIC CRYSTAL WAVEGUIDES

2.1. Basic Concepts and Designs

Introducing a 1D periodic perturbation in one or some rows of an otherwise-periodic PC will create a 1D periodic waveguide. If photons with frequencies within the PBG are launched into the defect region, they can (possibly) be guided by bouncing back and forth between the two surrounding PC regions. The 1D periodic perturbation can be increasing or decreasing the sizes of air holes. A special case of reduced-radius air holes is when the radius becomes zero and the holes are not etched. This design has a good theoretical performance and has almost the least sensitivity to fabrication imperfections. Note that the fundamental guided mode has most of its energy in the core and any small fabrication imperfections can result in considerable scattering. Besides, electromagnetic waves can be guided in this structure by both abovementioned PBG-guiding and also the conventional index-guiding (because of an effective index in the PC regions smaller than that of the core).

In general, if *n* parallel rows are removed, a PCW is obtained, which is referred to as a W_n PCW. If *n* is an even number, the structure will not be symmetric along the lateral direction and the concept of even and odd guided modes does not apply anymore. Some experimental studies have been done on large-core W_3 PCWs, since they can have better mode matching and coupling efficiency to outside sources. However, such waveguides

have more guided modes (with almost flat dispersions) in the PBG and are not useful in many practical guiding applications. Hence, we concentrate on W_1 PCWs in our study. Figure 1 shows the SEM image of a W_1 PCW connected to a conventional dielectric ridge waveguide.

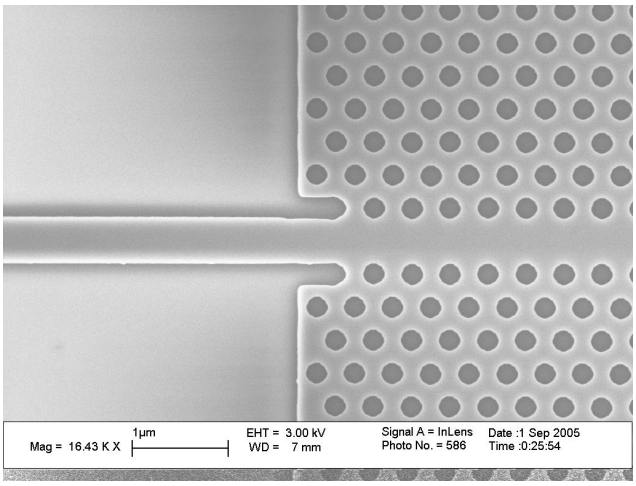

Figure 2.1. SEM image of a W_1 photonic crystal waveguide (right) fabricated on an SOI substrate and connected to a dielectric waveguide (left) fabricated on the same substrate

A W_1 PCW has usually two guided modes with even and odd parities in the frequency range corresponding to the PBG of the original PC as shown in Figure 2.1 [26] (Note that even and odd symmetries are defined here in the plane of periodicity and not in the transverse direction). 3D simulations [27] and also characterizations of both symmetric [24] and asymmetric [28, 29] PCWs defined on SOI substrates confirm the existence of guided modes similar to those predicted by 2D simulations. However, the differences between 2D PCs and PC slabs exist in the case of waveguides as well. Care must be taken in using the results of 2D simulations to interpret experimental results.

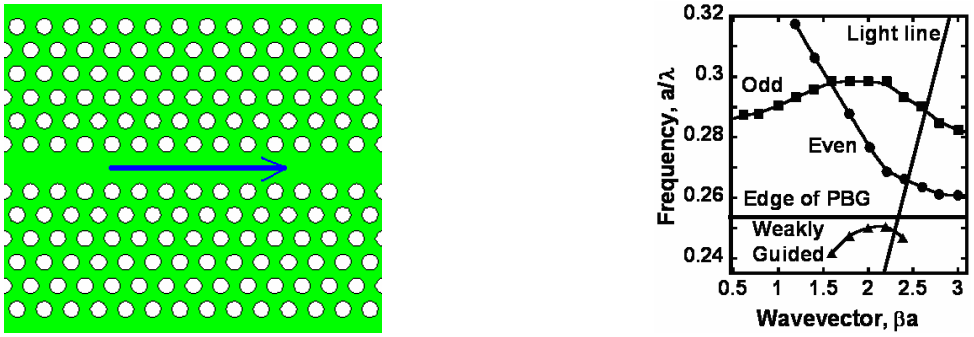

(a) (b)

Figure 2.2. (a) A triangular lattice photonic crystal waveguide made by removing (not etching) a row of air holes along the ΓK direction and (b) the corresponding dispersion diagram.

Only those parts of the modes that lie below the light line are confined in the slab and can be considered as guided. Some theoretical simulations have predicted quality factors of 400-1200 for guided resonances in PCWs above the light line [30]. As a result, the radiation mode of a PCW has a travel range of 40-300 periods before losing half of its power. This fact is usually observed in characterization of short PCWs with lengths close to 50 periods.

Also note that the edge of the irreducible Brillouin zone in a PCW (created along the ΓK direction) is π/a, whereas this number is $(4/3)\pi/a$ in the corresponding PC along the same direction.

2.2. Problems Associated with Photonic Crystal Waveguides

A PCW suffers from important problems, which make it inappropriate for practical applications in photonic integrated systems:

2.2.1. Modegap

A PCW is still a (1D) periodic structure. The very mechanism that gives rise to mode

splitting and bandgaps in the original crystal (i.e., DBR) results in similar phenomena in the PCW. The modes are folded and split at the edge of the Brillouin zone, and a *modegap* (a range of frequencies with no allowed guided modes) is created at lower frequencies of the PBG. Note that the modegap occupies the best part of PBG, which could have been used for guiding. Frequencies within the modegap are very far from the light line, and they are associated with the smallest density of states of radiation modes.

Note that there are Bragg resonances of different orders in PCWs and they result in several self-couplings of a mode and several modegaps at the edges of the irreducible Brillouin zone. There are also couplings between modes of different orders with the same parity [31]. As a result, the bandwidth above the modegap is limited by higher order modegaps in addition to other factors mentioned below.

2.2.2. Light Line Restriction

Modes at higher frequencies of the PBG lie above the light line and are not appropriate for guiding. If the structure is not in the form of a membrane, the light line will have a smaller slope and will intersect the dispersion diagrams at lower frequencies. So, the light line limitation is more important in such structures.

2.2.3. Multimode Nature

In many practical applications, it is desirable to have single-mode guiding to avoid even-odd couplings. The original PCW, however, is a multimode waveguide, if the entire PBG is considered. Limiting ourselves to the single-mode part of the PBG will further decrease the available guiding bandwidth.

2.2.4. Nonlinear Dispersion

While the nonlinear and flat dispersion of PCWs can be used (locally) to achieve *slow-light* [32] or lasing, it is not desirable in guiding applications. It is known that a pulse will experience distortions such as broadening and chirping in passing through a uniform waveguide (or optical fiber) operating at frequencies with nonlinear dispersion. A periodic waveguide will introduce similar distortions plus other effects originating from its periodic nature. In order to minimize such distortions, PCWs should be used in the linear regime of operation. It further decreases the available guiding bandwidth of PCWs.

2.2.5. Loss

Another important problem associated with PCWs is the much greater loss coefficient compared to that of a uniform waveguide of similar size. The unique properties of PCs and the confinement by PBG originate from the constructive/destructive interference of Bragg reflections from different layers of the structure. Small perturbations, as introduced by fabrication imperfections, "detune" this resonance behavior, and the resulting reflections will not be added with the expected phase relations. As a result, the PC cladding regions will not act as perfect mirrors for the waves propagating in the core of the waveguide and the energy of a (theoretically) guided mode can be coupled to some non-guided modes.

2.2.6. Coupling Efficiency

It is desirable to have a PCW with a coupling efficiency (to external dielectric

waveguides) close to unity at all frequencies of operation. However, coupling electromagnetic waves from a conventional dielectric waveguide to a periodic 2D waveguide is more complicated than the 1D case (transmission lines), where there are only transmitted and reflected waves. The difference between the transmitted and incident powers in PCWs can be accounted for by different mechanisms, which are mainly:

a) Back reflection into the input dielectric waveguide (as in the 1D case)

b) Back diffraction into the air region [33]

c) Propagation as a surface wave along the air/PC interface (in the lateral direction)

d) Leakage by coupling to the modes of the PC (at frequencies out of the PBG)

e) Out of plane leakage

f) Variations in the direction of power flow along the lateral direction and existence of power vortices [34]

2.3. Proposed Solutions for Dispersion Engineering

2.3.1. Changing the Waveguide Thickness:

One solution to increase the guiding bandwidth of PCWs is to decrease the width of the waveguide [35]. While the structure is still periodic and has modegap and mode flattening at some frequencies, it may have linear dispersion *throughout the PBG*. One may model the PCW with an equivalent slab waveguide and consider the effect of decreasing the width of the slab waveguide. The mode is shifted upward and the waveguide becomes multimode at higher frequencies. Using the terminology of band and

perturbation theories, by decreasing the dielectric in the structure, the modes are shifted towards the “air band” and away from the “dielectric band”, i.e., toward higher frequencies. So, it is possible to shift the flattening frequency out of the PBG by appropriate choice of the PCW thickness. The problem associated with such a method is that the overall periodicity of the PC is perturbed. It causes serious problems at bends, where different regions are actually different lattices with some offset with respect to each other.

2.3.2. Increasing the Radii of Air Holes Close to the Core

Another method introduced in the literature is to modify the sizes of the air holes close to the guiding region [36]. Increasing (decreasing) the sizes of these air holes will decrease (increase) the dielectric material in the structure and will push the modes toward the air (dielectric) bands, i.e., higher (lower) frequencies. Since the even mode has less energy around the air holes, it is not affected as the odd mode is. Hence, the shift in the odd mode is more than that in the even mode. This property has been used to make single-mode PCWs. Although this technique increases the size of the modegap, the idea can be combined with a novel perturbation reported here to provide two degrees of freedom in efficient optimization of PCWs.

2.3.3. Changing the Performance Index in Lattice Optimization

The common performance index used to optimize PCs has been the size of the (first) PBG. But, it is already known that only a small fraction of the PBG can be used for guiding. It has been demonstrated that it is possible to design the lattice to have a smaller

PBG, while the corresponding waveguides will have larger guiding bandwidths.

This is an important result, which should be taken into consideration in PC optimizations. However, once a lattice (even the "optimized" lattice) is given and a guiding bandwidth for the corresponding PCW is achieved, there may be some perturbations that still improve the dispersion and guiding bandwidth of the PCW. This technique may be considered as a complementary technique in dispersion engineering of PCWs.

2.3.4. Introducing a Phase Shift in the Two Rows Close to the Core

Introducing a phase shift between the two rows of air holes close to the core of PCWs removes the symmetry of the waveguide (about the centerline) and hence the even-odd symmetry of modes. Such a perturbation is not usually considered, for it mixes the even and odd modes of the structure. Parenthetically, this perturbation may be useful in applications where the (unperturbed) odd mode has a more promising behavior. The perturbed mode may still have the promising features of the (unperturbed) odd mode, in addition to the better confinement of the (unperturbed) even mode.

A more meaningful perturbation is when the two rows close to the core have the same phase, which is different from that of the other rows of the PC structure, as suggested by Yamada et al [37]. The resulting structure is still periodic with the same period as the original structure. While this perturbation in some cases results in single-mode PCWs, the resulting guiding bandwidth with linear dispersion is small. Mode intersection with the light line and mode flattening at the edge of Brillouin zone occur over a small bandwidth. However, this idea is useful for further tuning a PCW, which has already been

"optimized" using other degrees of freedom.

2.3.5. "Double-Trench" PCWs

This interesting design uses a channel waveguide with two PC regions in the cladding regions [38]. The resulting structure is still periodic with the same period as that of the cladding PCs. However, choosing appropriate values for the width of the slab and the size of the air gaps result in a better dispersion. Unlike the width-reduced designs, the overall periodicity of the lattice is not perturbed by this design.

Existence of air gaps results in more index contrast between core and cladding and more confinement of light in the dielectric core region. While this feature reduces the sensitivity to fabrication imperfections, it adversely affects coupling through the PC region and implementation of couplers. The main problem with this design is the existence of isolated regions that cannot be fabricated on thin films.

2.3.6. Embedding a Low-Index Slab

Guiding in this structure is merely based on PBG-guiding and there is no index-guiding. According to simulation results [39], the PCW is single-mode with linear dispersion below the light line over a large bandwidth; however, no experimental results have been reported. This structure is difficult to fabricate as part of a photonic integrated circuit. It also seems to be sensitive to fabrication imperfections in etching holes and also in forming the interface between dielectrics.

In the next chapter, we will introduce a perturbation mechanism, which uses the fundamental property of PCWs (periodicity and DBR) to engineer dispersion.

2.4. Concluding Remarks

We have studied the dispersion of PCWs and different schemes proposed for dispersion engineering in these structures. We will propose a new technique in Chapter 3 to improve the properties of PCWs and will discuss the method in detail

CHAPTER III

OPTIMIZATION OF PHOTONIC CRYSTAL WAVEGUIDES

3.1. Problem Definition and Performance Indices

Our goal is to perturb the PCW introduced in the previous section to achieve linear dispersion, high coupling efficiency, low loss, and single-mode behavior over a large bandwidth. Note that an accurate loss modeling in PCWs requires 3D simulations. However, we know that loss is a decreasing function of group velocity and that radiation modes have lower density of states at lower frequencies. So, linearizing dispersion especially at lower frequencies in our 2D simulations will reduce the loss coefficient.

3.2. The Proposed Perturbation Scheme

Mode couplings and modegaps are brought about by the periodicity of a structure and will vary by changing the period. How can this property be used to engineer the dispersion of a PCW? We consider a perturbation in the period of the two rows next to the guiding region by introducing a new periodicity, *a'*, in these two rows (as shown in Figure 3.1). The new structure comprises a "corrugated waveguide" with a periodicity of *a'* (referred to as *the a' structure*) and PC cladding regions with periodicity of a (referred to as *the a structure*). The goal is to find a value of *a'*, for which the fundamental mode of the *a'* structure has a linear dispersion in the frequency range determined by the PBG

of the *a* structure. In practice, the *a* and *a'* structures are coupled to each other. So, they cannot be treated separately and more tuning of a' may be needed. However, this conceptual discussion helps to understand the approach [26].

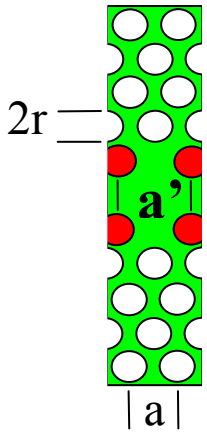

Figure 3.1. A biperiodic PCW with a different period in the two rows close to the core.

Introducing this perturbation in more rows (for example two rows on each side of the waveguide core) will result in a larger defect size and a larger effective width of the waveguide. It makes the waveguide multimode with highly nonlinear dispersion. It is why we use just one row on each side for this perturbation.

Perturbation in period can also be achieved by other techniques. The most familiar one is chirping. Our simulations have not shown considerable improvement in transmission of PCWs after chirping. Also note that chirping a PCW makes it very sensitive to length and the holes may start to overlap at some point.

Randomizing the holes close to the guiding region can also result in high transmission. However, it will result in an inhomogeneous system in which there may be no meaningful phase relation between wavelets scattered off different air holes.

3.3. Transmission of Perturbed Straight Waveguides

Unless otherwise stated, all PCWs are created by removing one row of air holes along the ΓK direction in a 2D triangular lattice PC. The PC under study has a length equal to 14 lattice constants, an effective dielectric constant of 7.9; a periodicity of *a* equal to the size of 24 FDTD grid cells, a normalized radius of r/a = 0.3 and is excited with TM polarization. By using FDTD, the PBG of the structure is found to be between the normalized frequencies 0.253 and 0.320. The PCW under study is connected to an input slab waveguide with an embedded Huygens source, which radiates energy only in one direction. The structure is surrounded by Perfectly Matched Layers (PMLs) [40] to avoid reflections. For the measurement of power transmission, we integrate the Poynting vector on a surface normal to the longitudinal direction, as shown in Figure 3.2 (b). The middle of this hypothetical surface coincides with the axis of the PCW. A similar calculation is done in a structure with no PC region and with the slab going all the way to the right of the structure. The power calculated in the second system is the total incident power. The normalized power transmission of the PCW is the power calculated in the first system divided by that calculated in the second system [26, 41].

The Poynting vector changes sign along the lateral (y) direction. While power flows in the forward direction in the core of the waveguide, it forms vortices around air holes and flows backward at some parts of the cladding regions [34]. In a dielectric waveguide, however, the Poynting vector associated with an even mode is in the direction of propagation both in the core and in the cladding regions. So, care must be taken in defining the size of the output surface in Figure 3.2 (b) and in interpreting the results. Some of the (potential) numerical errors in calculation of transmission spectra of PCWs

are as follows:

i. Having polygons rather than circles because of space discretization

ii. Inappropriate "effective width" considered for the PCW

iii. Sampling a triangular lattice (with a 6-point symmetry) in a Cartesian coordinate system (with a 4-point symmetry) [42]

iv. Insufficient simulation time for modeling a quasi-stationary state

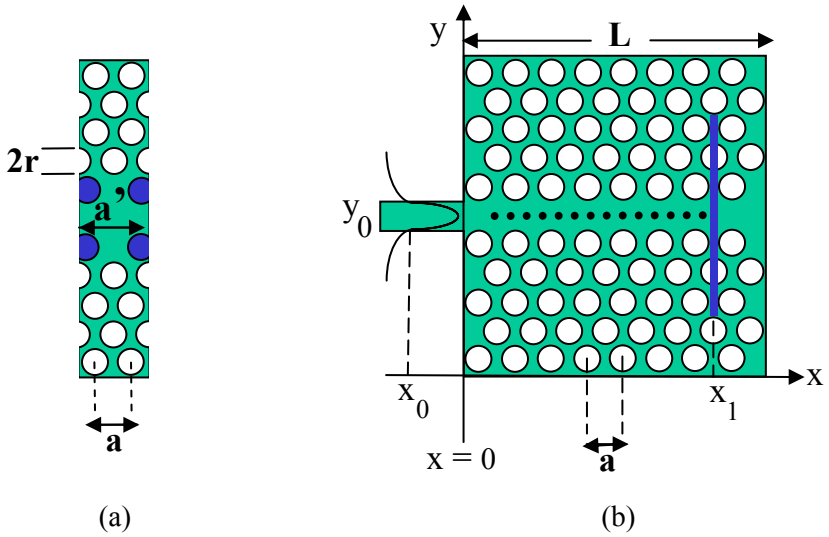

Figure 3.2. (a) A biperiodic PCW made by removing one row of air holes from a triangular lattice PC of air holes in the dielectric and introducing a new periodicity in the layers next to the guiding region. (b) The basic structure used for the analysis of PCWs. A pulsed Huygens source is placed in the slab waveguide at $x = x_0$ and the corresponding field is calculated at all points in the same horizontal line along the guiding direction (x). For calculation of power transmission spectrum, the Poynting vector is calculated and integrated over a surface at $x = x_1$.

The results of transmission calculations have been plotted in Figure 3.3. It is seen that the edge of the modegap is shifted toward higher (lower) frequencies and even out of the PBG by decreasing (increasing) the periodicity. Note that for $a'/a = 0.70$, it is possible to have guiding with high transmission coefficients over the whole PBG.

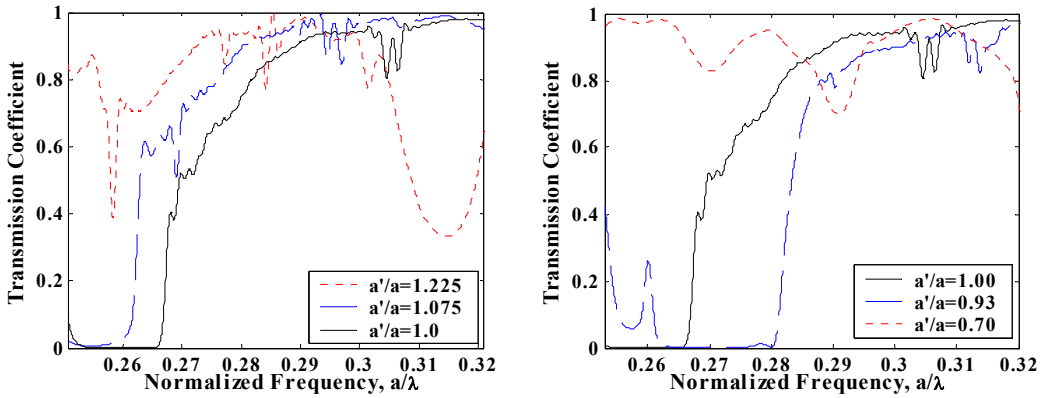

(a) (b)

Figure 3.3. The evolution of mode flattening and DBR as the period changes: power transmission coefficient at x_1=14a for the PCW in Figure 3.2(a) for (a) increasing the period and (b) decreasing the period.

The results shown in Figure 3.3 are promising and as expected. A pattern is observed in the position of the edge of transmission as the second period changes. One can specifically note the high transmission coefficient at lower frequencies and within the modegap of the original PCW (a'/a=1.00). High transmission in straight waveguides is a necessary, but not a sufficient condition for applications in photonic integrated systems. We then evaluate the performance of bent waveguides with and without perturbation in period.

3.4. Transmission of Perturbed Bent Waveguides

Figures 3.4 (a) and 3.4 (b) show conventional and biperiodic PC bends, respectively. The bends are created by cascading two 120° bends in the structure. The period of the air holes in the two rows next to the guiding region of the biperiodic structure is $a' = 0.7a$, where a represents the lattice constant of the original PCW. Corresponding transmission spectra have been shown in Figure 3.4 (c). The horizontal axis shows the normalized

frequencies in the photonic bandgap (PBG: $0.253 < a/\lambda < 0.32$). The waveguide modes in the upper half of the PBG lie above the light line, where radiation and leaky modes co-exist. So, we mainly concentrate on the behavior of the structures in the lower part of the PBG (i.e., $a/\lambda < 0.28$).

Figure 3.4 (c) shows that the high-transmission window corresponding to the conventional bend has been widened, flattened, and increased in amplitude in the corresponding biperiodic bend [43]. Besides, there is a new high-transmission window in the spectrum of the biperiodic bend at the lower portion of the PBG, where the conventional bend has essentially zero transmission. These frequencies correspond to the modegap of the conventional PCW, where there is no guided mode.

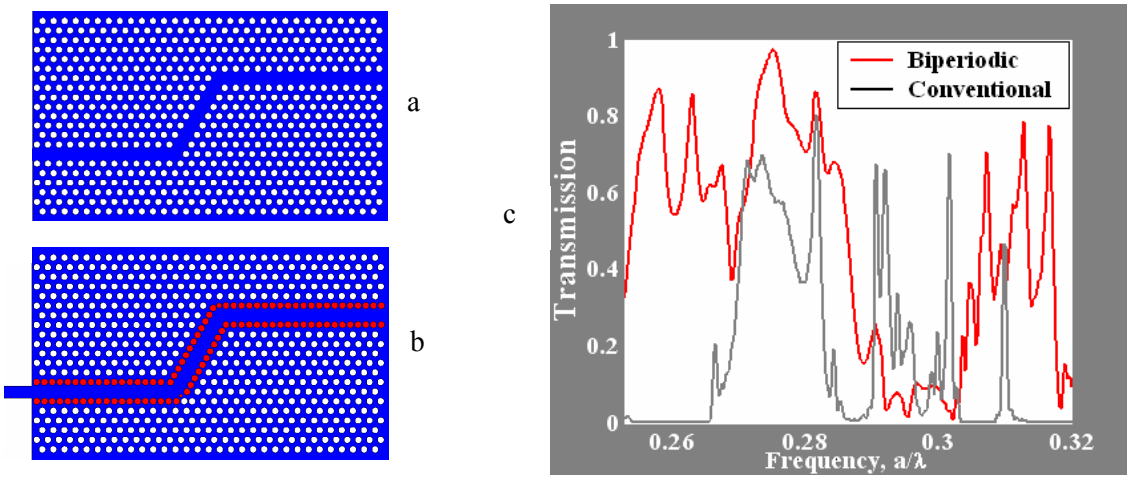

Figure 3.4. (a) A conventional and (b) a biperiodic bend in a 2D photonic crystal structure. The second period of the biperiodic structure has the normalized value of a'/a=0.7. (c) The transmission coefficient of the two bends in parts (a) and (b) with a high transmission of the latter and a modegap of the former at low frequencies.

3.5. Other Optical Functionalities

Biperiodic PCs not only can guide electromagnetic waves along straight and bent waveguides, but also can couple waves from one waveguide to another. This important

property can be used in realization of optical filters and separation of different channels. Coupling occurs from biperiodic PCWs to both conventional and biperiodic PCWs. Note that the large bandwidth obtained using a biperiodic PCW is not necessary in all regions of a photonic integrated system. A waveguide associated with a specific channel does not need a large bandwidth and can also be realized using a conventional PCW. Even if narrowband dispersion linearization is needed, it can be achieved by perturbations that do not change the period (like changing the radii of air holes close to the guiding region). Wave coupling still occurs because of evanescent coupling between conventional and biperiodic PCWs. Figure 3.5 shows a typical coupling in these structures. This Figure corresponds to two parallel biperiodic PCWs (a'/a= 1.0833) operating at the normalized frequency of a/λ=0.25974. As in conventional PCWs, tuning air holes or other schemes can be used to improve the coupling.

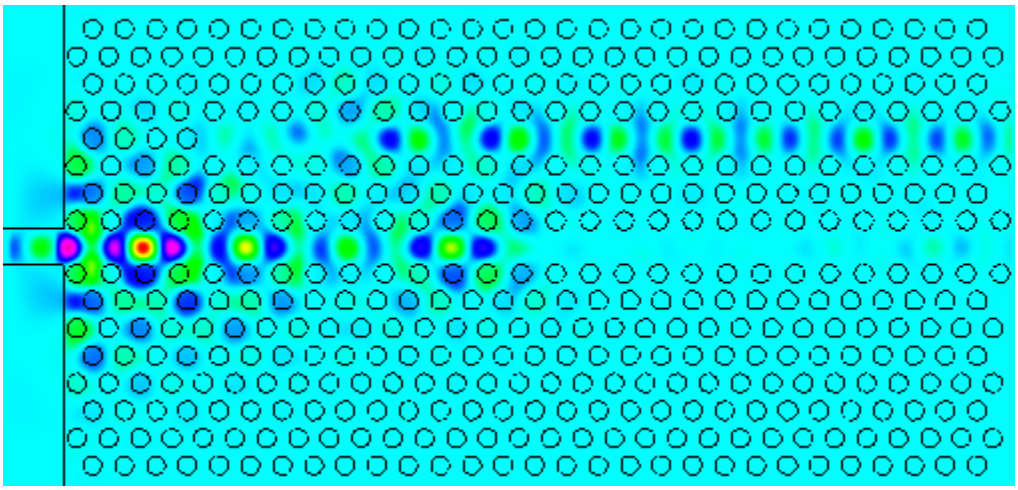

Figure 3.5. Power Coupling from one biperiodic PCW to another.

3.6. Modal Analysis of Perturbed Structures

What is the origin of these modes and how does the perturbation in period affect

modal characteristics of the PCW? The modes propagating in uniform or periodic waveguides are characterized by an eigenvector (field) and an eigenvalue (propagation constant). We have seen how the TM transmission spectrum (the power carried by the magnetic field) changes as we perturb the period of a PCW. Is it also possible to see a similar evolution pattern in the eigenvalue (propagation constant) space?

Biperiodic PCWs have an interesting and a relatively simple behavior in the *k*-space (wavevector space) that will be discussed in Section 3.9. However, we first try to develop a general technique to characterize arbitrary "nonperiodic" structures.

3.6.1. Dispersion Calculation Using Spatial Fourier Transform (SFT)

We first calculate the electromagnetic field distribution in the waveguide under study using FDTD and save the values of fields at some points along the longitudinal direction as shown in Figure 3.2 (b). We then take a Fourier transform with respect to time to have the spectral representation of the field. Knowing the spatial distribution of a field at a given frequency ($H_\omega(x)$), we can easily find the *k*-space representation by taking the spatial Fourier transform with respect to the space coordinate variable ($H_\omega(k)$). The field may have some energy over a continuum of modes that can be excited at waveguide junctions, but cannot propagate over a large distance in the waveguide. But, the energy of the field is mainly concentrated in one or some resonances, which represent the modes (and their Floquet components, if any) supported by the waveguide.

We will use this property to monitor the distribution of field energy (at a given frequency) over different spatial frequencies [41]. If similar resonances are observed, it will be meaningful to attribute (quasi) modes to such a structure. Furthermore, the

positions of such resonances will specify the dominant spatial frequencies or propagation constants. Plotting these propagation constants versus frequency will result in the "dispersion diagram".

Figure 3.6 shows a typical spatial Fourier Transform (SFT) spectrum of a biperiodic PCW with a'/a=0.7 at normalized frequency of a/λ=0.257. We have also shown the SFT of a single exponential function $f(x) = e^{j\beta x}$, with β=1.236π/a, which corresponds to the peak of the SFT spectrum of the biperiodic PCW at a/λ=0.257. The sampling parameters in the two SFT calculations are the same. The existence of a single SFT spectral peak for the PCW and the equality of the widths (and the shapes) of the two SFT spectra in Figure 3.6 confirm that it is valid to assign a single propagation constant to this biperiodic PCW.

For the sake of comparison, we have also shown a similar SFT of the conventional (a'/a=1) PCW in Figure 3.6 with a peak at a different value of spatial frequency k. The similarity between the shapes of the SFTs of the fields in the periodic and biperiodic PCWs is another indication of the existence of a well-defined propagating mode in this biperiodic PCW.

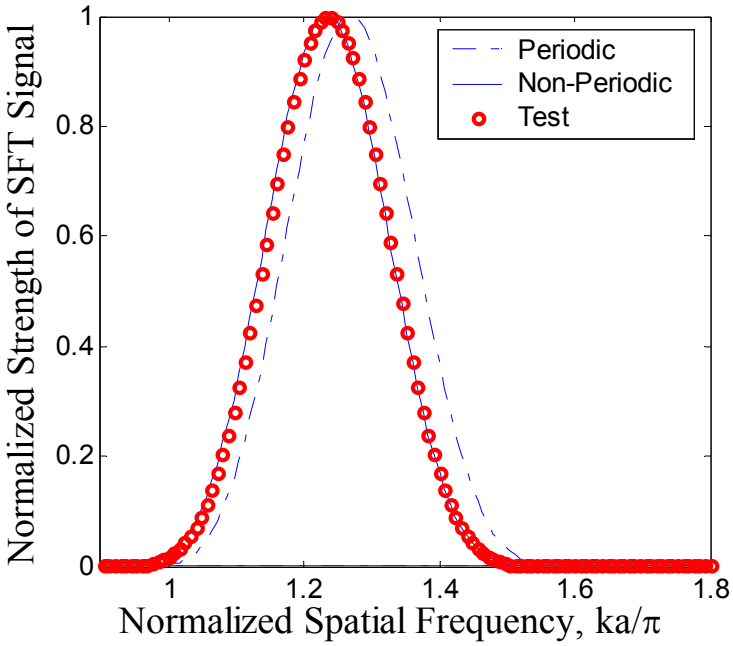

Figure 3.6. Normalized strength (magnitude squared) of the SFT of the magnetic field of the fundamental TM mode for a periodic and a biperiodic PCW at different frequencies and also the SFT of a complex exponential function

Also, note that in both cases, a single "Floquet" component carries most of the energy of the guided mode. It justifies truncating the plane wave expansion of the mode at these frequencies and using one (or in general a few) component(s) in the forward and in the backward directions as a good approximation. Note that the function $H_\omega(x)$ is a complex function and hence the magnitude of $H_\omega(\mathrm{k})$ is not an even function in general. So, a peak at positive spatial frequencies does not necessarily imply a similar peak at negative frequencies. Identification of Floquet components excited by the source is another important application of the SFT technique.

3.6.2. Dispersion of Biperiodic PCWs

By finding dominant spatial frequencies at different temporal frequencies, the

dispersion diagrams can be plotted. Figure 3.7 shows the evolution of the dispersion of the fundamental mode in the PCW under study. It is seen that the edge of the modegap is shifted toward higher (lower) frequencies and even out of the PBG by decreasing (increasing) the periodicity. Not only the trend in mode evolution, but also the exact positions of the flattening frequencies are in good agreements with the results from transmission diagrams. Similar correspondence has been observed between transmission and the so-obtained dispersion of chirped PCWs.

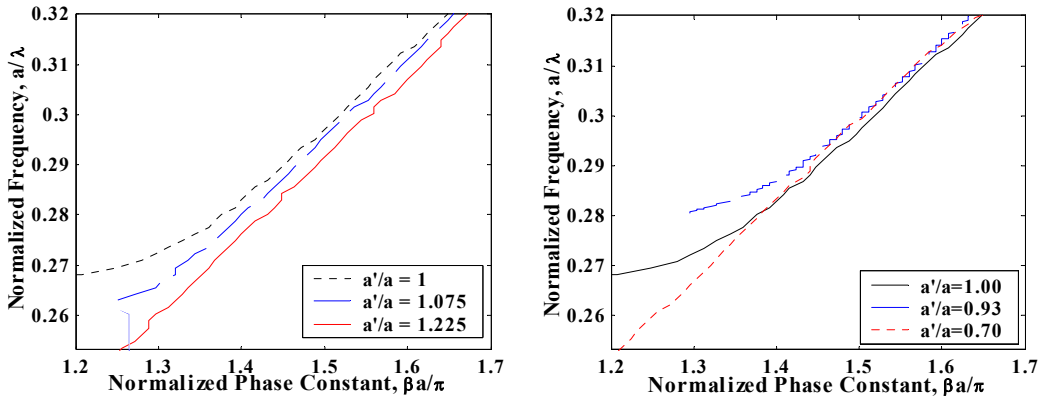

(a) (b)

Figure 3.7. The evolution of dispersion diagram as the period changes: Dispersion diagram of the fundamental TM mode for the PCW in Figure 3.2 with a) increased periods and b)decreased periods.

3.6.3. Alternative Methods of Dispersion Calculation

Methods relying on the periodicity of a PCW such as PWM cannot be used (at least directly) to analyze PCWs with perturbed periods. The conventional coupled-mode theory cannot be used, either.

Coupled mode theory is a powerful and popular technique to study the effect of "small perturbations" in waveguides. The starting point for the coupled-mode formalism is using the Lorentz reciprocity relation [44]. The conventional coupled mode

formulation (for uniform waveguides) is obtained by integrating this equation over the cross section of the waveguide under study. The fundamental assumption in this formulation is a uniform cross section along the longitudinal direction of the waveguide.

The coupled mode formalism can be extended to PCWs by integration over a unit-cell. There is also a discrete coupled mode theory for PCWs, which has a simple formulation and interesting applications such as incorporating the effect of material dispersion in calculating the dispersion of PCWs [45]. However, the fundamental assumption in both cases is periodicity of the structure and existence of a unit-cell. So, these methods cannot be applied to biperiodic PCWs (not to mention that the perturbation in biperiodic PCWs is not necessarily "small").

There is also a more complicated formulation of coupled mode theory in PCWs, which considers position-dependent ("instantaneous") propagation constants [46]. This method is mainly useful in driving the condition for adiabatic tapering in PCWs and may be applied to chirped PCWs with small perturbation. It is not easy to apply or generalize this method (based on first order perturbation theory) to model large perturbations in biperiodic PCWs.

Finally note that the information provided by both the dispersion diagram and the density of states (DOS) are needed to have a complete picture of modes. The evolution of local DOS as a function of perturbation in period is the subject of an ongoing research.

3.7. Single-Mode Large-Bandwidth Photonic Crystal Waveguides

Perturbing the period affects mode couplings and mode gaps. So far, we have concentrated on useful consequences of periodicity perturbation on the even mode. But

the fact is this perturbation can remove the modegap of the odd mode, too. As a result, there will be guided odd modes over a large frequency range in the PBG, even at frequencies that the original PCW did not support odd modes. The large mode gap for the odd mode at lower frequencies of the PBG is brought about by coupling between two odd modes with different orders [31]. Perturbing the period affects the coupling between these two modes and extends those two odd modes over a large frequency range. Figure 3.8 shows the field profiles of the odd mode of the biperiodic PCW with a'/a=0.7 (having the largest bandwidth for even mode), at two frequencies below and above the PBG, where the original PCW was single-mode.

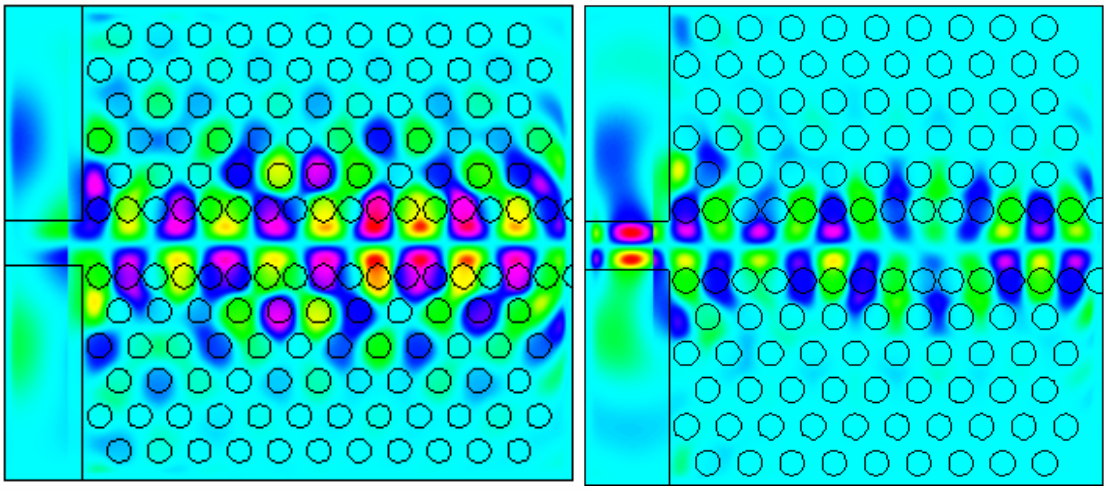

Figure 3.8. Field profiles of the odd mode in a biperiodic PCW at normalized frequencies of 0.257 (left) and 0.311 (right) calculated using FDTD simulations.

In order to resolve this issue, we note that dispersion engineering will be easier if the slope and offset of modes can be modified almost independently. Perturbing the period can change the slope of the even mode significantly [26] and perturbing the radius can introduce a large offset in the position of the odd mode [23]. Of course both perturbations affect both modes, but we hope that appropriate perturbations in period and radius can

improve the performance of the even mode without bringing the odd mode into the picture.

We have simulated the transmission of even and odd modes in many PCWs in which the radius and period (of the air holes close to the core of the waveguide) have assumed different values. Given a pair of (r', a'), we consider the fraction of the frequency range between the lower edge of the PBG and the light line intersection with dispersion that has guided even modes (transmission greater than 10%), but no guided odd modes (transmission less than 0.2%). We limit the range of variations of r' and a' to the values that can be actually fabricated using state-of-the-art fabrication tools. This range approximately covers $2/7 \leq r'/r \leq 10/7$ and $a'-2r' \geq a/6$. Our approach is to allow both parameters to vary and find the single-mode guiding bandwidth below the light line for each set of (r',a'). Once we find PCWs with large bandwidths, we can also investigate the linearity of their dispersion and their coupling efficiency to an input slab waveguide to find the optimal PCW. The results of this exhaustive search are shown in Figure 3.9 (b) as the colored map of the single-mode guiding bandwidth in the two-dimensional design space of r'/r and a'/a. To assure single-mode guiding, we calculate the transmission spectra of both even and odd modes through a long PCW (L=30a in Figure 3.2 (b)) and consider the frequency range with high transmission of the even mode and negligible transmission of the odd mode. The single-mode guiding bandwidth of any structure has been normalized to the size of the frequency range of interest ($\Delta(a/\lambda)$=0.268-0.253=0.015). The points in dark red designate good choices of r' and a'.

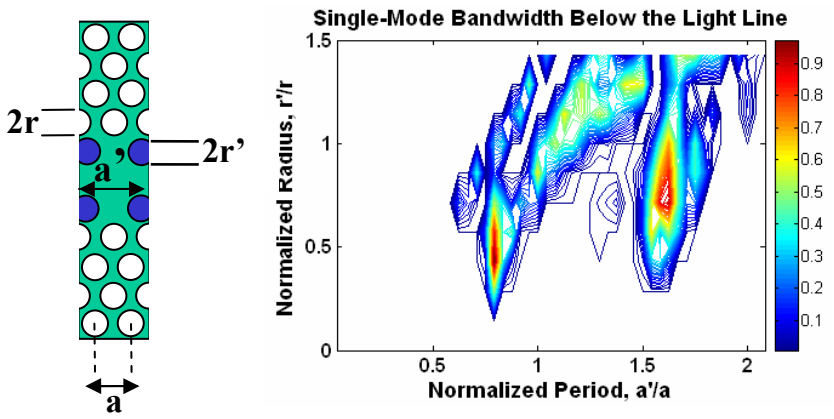

(a) (b)

Figure 3.9. (a) A section of a biperiodic PCW and (b) the fraction of the frequency range between the lower edge of the PBG and below the light line with high transmission of the even mode and low transmission of the odd mode for different pairs of r' amd a'.

Figure 3.9 clearly shows that the single-mode guiding bandwidth of the original unperturbed PCW (*r'/r,a'/a*)=(1,1) is considerably smaller than those of many biperiodic PCWs. As an example, the transmission spectra of two PCWs with (*r'/r,a'/a*)=(1,1) (the original PCW with no perturbation in periodicity or radius) and (*r'/r,a'/a*)=(3/7,19/24) for even and odd excitations are shown in Figures 3.10 (a) and 3.10 (b), respectively.

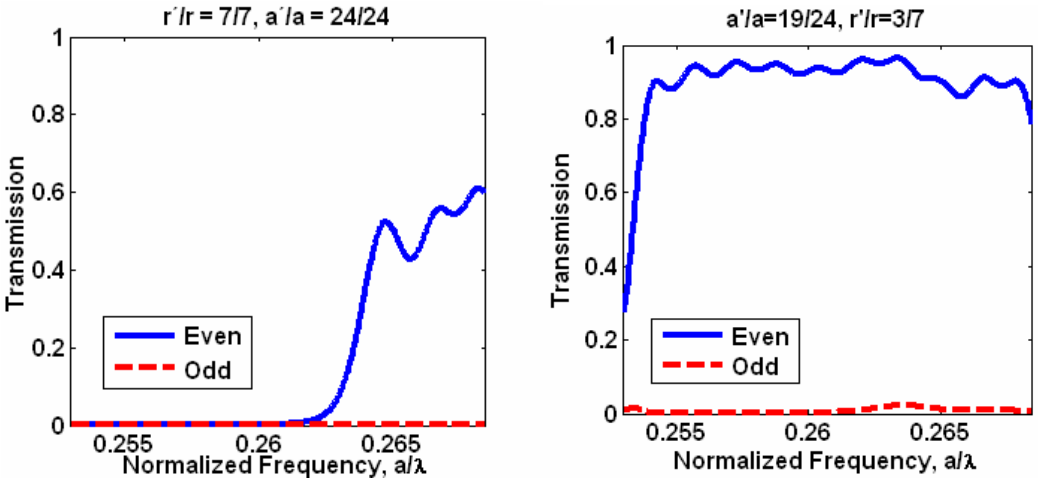

(a) (b)

Figure 3.10. The transmissions of the even and odd modes in the frequency range above the lower edge of the PBG and below the light line for a) the conventional PCW (*r'/r* , *a'/a*)=(1,1) and b) a biperiodic PCW with (*r'/r* , *a'/a*)=(3/7,19/24). The biperiodic PCW has a larger single-mode guiding bandwidth with much better coupling to the input slab waveguide.

It is important to know how the even mode evolves as the PCW is perturbed from the (r'/r,a'/a)=(1,1) point to the optimal (r'/r,a'/a)=(3/7,19/24) point and whether the dispersion becomes more linear. The dispersion diagrams of the even mode (calculated using the SFT technique) for the two abovementioned cases are shown in Figure 3.11. It is clear that over the normalized frequency range of $0.253<a/\lambda<0.268$, the PCW has linear dispersion. Furthermore, this guiding bandwidth occurs well below the light line, which results in low-loss propagation.

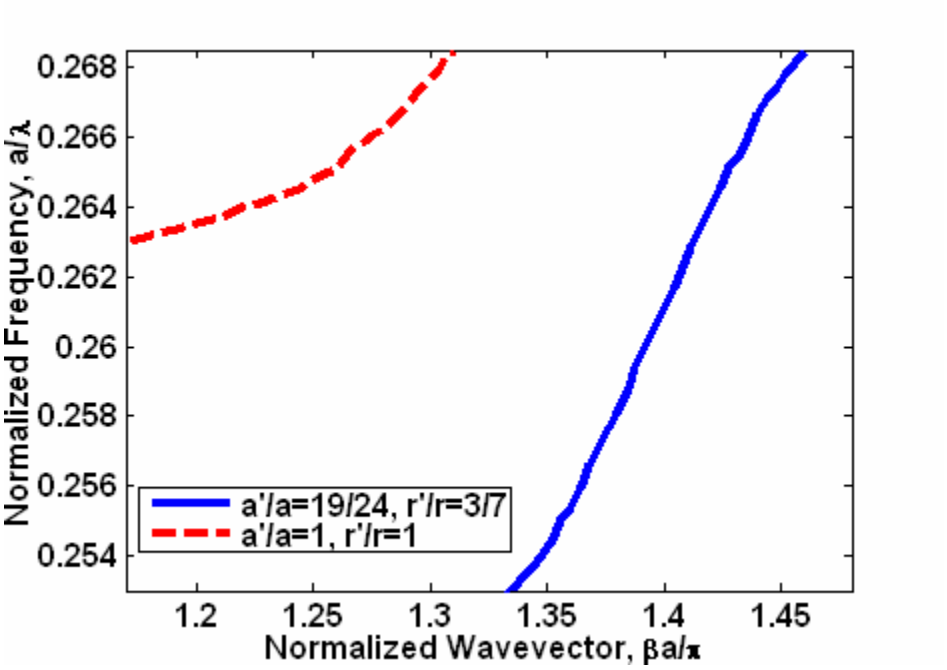

Figure 3.11. The dispersion diagrams of the even TM modes of the original PCW ($r'/r=a'/a=1$) and a biperiodic PCW ($r'/r=3/7$, $a'/a=19/24$). Note that the guiding bandwidth of the biperiodic PCW has been extended to the entire frequency interval within the PBG and below the light line. The dispersion is almost linear over the entire guiding bandwidth ($0.253<a/\lambda<0.268$) in this biperiodic PCW.

3.8. Experimental Results: The Record Loss of Biperiodic PCWs

One of the most important problems associated with PCWs is loss, which is always much higher compared to that of a ridge waveguide. For example, using the state of the

art CMOS line at IBM, McNab et al reported a PCW with a record loss of 2.4 dB/mm. However, this value is still almost an order of magnitude higher than the loss of a ridge waveguide (0.35 dB/mm) fabricated using the same facility.

We demonstrated a large guiding bandwidth and a small loss coefficient by using a biperiodic PCW [47]. An SEM image of the biperiodic PCW has been shown in Figure 3.12. A propagation loss as low as 2 dB/mm was reported for the first time in a PCW fabricated using commonly available fabrication equipments (EBL and RIE). We also reported the propagation loss of 3dB/mm or less over a bandwidth of at least 60 nm, which was 75 times the channel spacing of DWDM signals (0.8 nm) and 1.5 times the bandwidth of the C-band (1525-1565nm). The value of 3 dB/mm is about the same as the loss of a dielectric ridge waveguide fabricated using the same equipment.

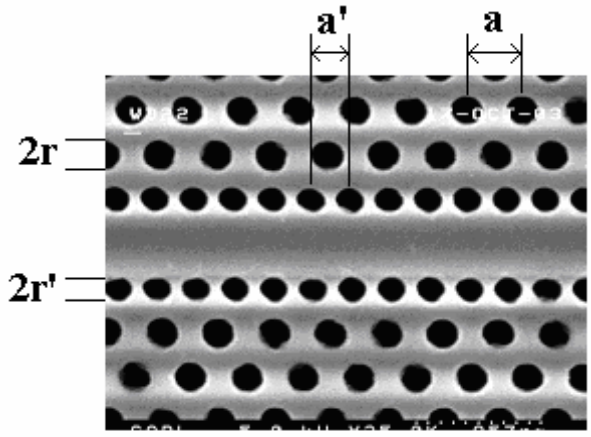

Figure 3.12. SEM view of a biperiodic photonic crystal waveguide. The radius and the period of the air holes in the two rows next to the guiding region are a'=0.7a and r'=0.25a, respectively. The lattice constant is a=420nm.

The samples were fabricated on a silicon on insulator (SOI) substrate with a Si slab of thickness t=260nm, separated from the Si substrate by a 1-micron layer of SiO_2. The

PCWs were patterned with direct write e-beam lithography and etched using reactive ion etching using $CHF_3/He/O_2$ and HBr chemistry.

The large transmission coefficient at lower frequencies ($0.268< a/\lambda <0.280$) in the biperiodic PCW is caused by shifting the DBR frequency to higher frequencies. The low transmission at higher frequencies ($a/\lambda >0.285$) is due to coupling of the guided mode to the radiation modes (above the light line). Figure 3.13 (a) shows equal normalized transmission of two biperiodic PCWs with lengths of 50*a* and 400*a*, where *a* is the lattice constant.

Normalized transmission of a PCW is obtained by dividing the transmission of that waveguide to the transmission of a reference ridge waveguide. The main goal of this normalization is to eliminate spectral features brought about by the source, the characterization setup, and on-chip elements connected to the waveguide [47]. This normalization will be the same for short and long waveguides and will not affect the measured loss coefficient. This normalization will not affect the position or size of modegaps, either. The width of the reference ridge waveguide is usually chosen to be equal to the effective width of the PCW, which can be the vertical distance between two air holes on the two sides of the waveguide core. The choice of an appropriate reference waveguide is more important and critical in dispersion measurements and will be discussed in section 4.2.3.2.

Also under study eliminate spectral features of the source, It is seen that even in the linear scale, the transmission curves coincide with each other in the frequency range of $0.268< a/\lambda<0.28$, which implies a very small loss coefficient. This small loss coefficient corresponds to a large bandwidth of about 60nm at optical communication wavelength.

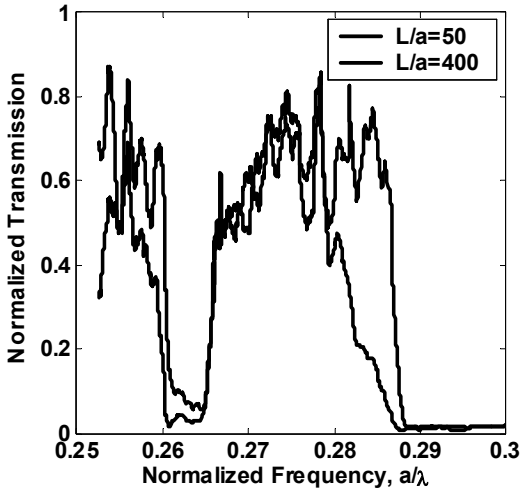

Figure 3.13. The normalized power transmission through a biperiodic PCW (a'=0.7a) with two different lengths at different frequencies. The low-loss region corresponds to 60nm in the optical communication wavelengths.

To measure the loss accurately, the measurements were repeated in several PCWs with lengths between 50*a* to 400*a*. Variations of the measured normalized power transmission through a conventional and a biperiodic PCW with length, *L*, at a low-loss frequency (a/λ =0.275) is shown in Figure 3.14. Fitting an exponential function to the measured data (as shown in Figure 3.14) results in (absolute) loss coefficients of 2.0 dB/mm and 66.4 dB/mm for the biperiodic and conventional PCWs, respectively.

The accuracy of these loss measurements is about 20%. The measurements were repeated on the biperiodic PCW for all frequencies in the range of $0.268< a/\lambda <0.280$ and a loss coefficient smaller than 3 dB/mm was obtained. Note that the loss of the ridge waveguide is about 3.5 dB/mm. This is, to the best of our knowledge, the first report of a PCW having a loss close to that of a dielectric ridge waveguide with similar width fabricated on the same substrate.

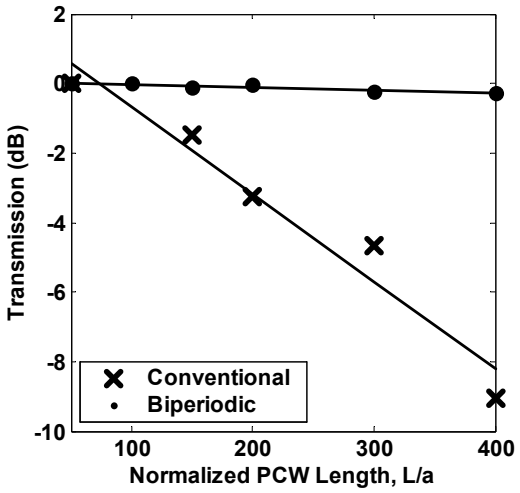

Figure 3. 14: Variations of power transmission through the biperiodic and the conventional PCWs described in Figure 13 at the normalized frequency of a/λ=0.275 for the biperiodic PCW and at a frequency with highest transmission for the conventional PCW.

3.9. Qualitative Description of Mode Coupling

Although coupled-mode theory is not easy to use for quantitative results, it is helpful in understanding the underlying physics of wave propagation and reflection in these structures in a qualitative argument:

3.9.1. Distribution of Spatial Frequencies

A biperiodic PCW is comprised of two regions: 1) two PC regions with similar periods (*a*) and 2) a set of two rows of air holes with another period (*a'*). Each region generates a set of Floquet components upon electromagnetic excitation. Any Floquet component corresponding to one periodic system will be diffracted by the other periodic system and as a result there will be a *double diffraction* in the system [48]. In other words, wave propagation in biperiodic PCWs is described by discrete spatial components and not a continuum of *k*. This is consistent with the properties of the peaks seen in the

SFT spectra.

3.9.2. Resonance Condition

A resonance DBR condition occurs when a forward propagating wavevector is equal to one of its backward-propagating Flouqet components (self-coupling in the single-mode case) or components corresponding to another mode with the same symmetry (cross coupling in the multimode case, which can be):

$$\beta_1 = \pm\beta_2 + m(2\pi/a) + n(2\pi/a')$$

For $\beta_1 = \beta_2 = \beta$, the equation will reduce to

$$\beta = m(\pi/a) + n(\pi/a')$$

3.9.3. Modegaps

A resonance condition does not necessarily imply a modegap:

3.9.3.1: n=0

There will be a DBR resonance in claddings, but waves can still propagate in the core and in the two rows of air holes close to the core. It can result in more confinement of the mode and not a modegap.

3.9.3.2: m=0

Since the energy of an even mode is mainly confined in the core, the structure will have an ordinary modegap (with zero transmission even for small lengths) because of DBR resonances in the core. In other words, the structure has an effective period of *a'*,

and the trends shown in Figures 3.3 and 3.7 correspond to the case where m=0 and β varies almost as 1/a'. We have also considered a PCW which has a period of a' in all rows. It shows the same DBR frequencies as the biperiodic PCW with a' just close to the core.

3.9.3.3.: $m \neq 0$ and $n \neq 0$

A weak coupling occurs between the core and cladding; this coupling is enhanced as the length of the structure increases. Small fluctuations in the high transmission regions will become dips as the length increases. For a given length of the waveguide, the effect is more clear, when the ratio a'/a is equal to the ratio of two small integer numbers. In such cases, 1) the overall structure is periodic and 2) the length of the waveguide is several times the overall unit cell. Simulations show that such a structure is different from other perturbed structures. It features two low-transmission regions; one with zero transmission in an anticipated frequency range (by comparing with other perturbed structures) and another bandwidth with low (but nonzero) transmission.

Given the finite resolution of fabrication systems and finite word-size of digital computers, a'/a cannot be an irrational number; neither in simulations, nor in practice. So, biperiodic PCWs *would* always become periodic if extended enough. Suppose $a'/a=M/N$, where M and N are integers and M/N has been reduced to its lowest term. The overall period of such a system is $a_{new}=Ma$. However, a biperiodic PCW will not have a modegap, if the length is smaller or even a few times the overall period.

3.9.4. Design Methodology

Consider a relatively short biperiodic PCW, so that the modegap associated with DBR resonances in the core is observed, but DBR resonances between the core and cladding are not observed. Introduce arbitrary perturbations in *a'* (and *r'*, if needed) to achieve the required performance. Now, modify *a'* by a small amount so that *a'/a* approaches an irrational number, i.e., *M* and consequently a_{new} become very large.

For example if *a*=400nm and a good performance is observed in a short biperiodic PCW with *a'*=450, then *a'/a*=450/400=5/4 and a_{new}=5*a*. So, if the PCW is 5*a* or a few times this value, there will be strong couplings between the core and cladding regions. However, if we choose *a'* to be 449nm (or 457nm or 443nm to account for fabrication resolution), then a_{new} will be 449*a* (or 457*a* or 443*a*), while the modegap originating from DBR resonances in the core is practically unchanged. Here we have chosen prime numbers close to 450, but any other number, which results in a large *M* is also good.

One may argue that the difference between 450nm and 449nm is very small and within the resolution of nanolithography systems. This point is valid and it is why we would chose prime numbers (457 or 443 rather than 449), which are relatively far from the original number (450). However, one usually fabricates PC structures that are tens of unit cells long. Two PCs fabricated with close periods, but with relatively large numbers of periods, will be distinguishable. Also note that fabrication errors usually occur in the size of the air holes (because of electron back scattering, for instance), and the inter-hole spacing has a relatively good accuracy.

3.10. Concluding Remarks

In summary, we have introduced a new method for dispersion engineering in PCWs and have shown theoretical and experimental results. The experimental results are obtained using the conventional technique of transmission measurement. A more complete characterization will also include dispersion measurement of PCWs. We will discuss different techniques of dispersion measurement in PCWs and will show the results of the first real-time dispersion measurement in PCWs in Chapter 4.

CHAPTER IV

REAL-TIME SPECTRAL PHASE MEASUREMENT

4.1. Dispersion Measurement in PCs

Characterization of PC structures is usually limited to measurement of transmission coefficients, i.e., amplitude measurements. A few experiments have also reported "phase measurement" in PCs at near infrared wavelengths using coherent wideband femtosecond laser pulses. Rosner et al. used short pulses to study the dispersion of three dimensional (bulk) photonic crystal structures using spatial interferometry [49]. Netti et al. used a time domain technique to measure group velocity in silicon nitride PCWs [50]. Balistreri et al. used a heterodyne scheme and near field microscopy to measure phase and group velocities of photonic crystal structures [51].

The aforementioned phase measurements have different features and can be contrasted in different ways:

4.1.1. Bulk vs. Waveguide

3D PCs and 2D PC slabs both feature nano-scale dimensions. However, corresponding characterizations are very different. Alignment of 2D PC slabs and maintaining this alignment is more challenging than characterization of 3D PCs, since the latter simply behaves as (anisotropic) bulk.

4.1.2. Time-Domain vs. Frequency Domain

"Phase measurement" may refer to *spectral phase* measurement, which is done by *frequency-domain* techniques or may refer to *group delay*, which is done by *time-domain* techniques.

The result of a time-domain technique may just be one number; the group velocity or group delay at the center wavelength of the source bandwidth. However, frequency-domain techniques (and also some time-domain techniques) provide the information of phase or group velocity over the entire spectrum of interest.

If the spectral phase function is written as a Taylor series expansion around the center wavelength (of the given bandwidth), the coefficients of such a series are related to group delay, chirp, and other time-domain parameters.

4.1.3. Local vs. Cumulative Dispersion

Using near-field optical techniques, it is possible to measure spectral phase functions at different points of a PCW or other nanostructures. These measurements provide more information (spectral and spatial evolution of phase). They can also provide a simple and reliable phase reference at any frequency, which can be the phase measured at the first point.

However, conventional techniques using *one* output signal to measure phase, may face difficulties in defining a reference phase at any frequency and taking into account the phase shifts introduced by different dispersive elements attached to the sample under test and contributing to the total phase.

4.1.4. Redundancy of Information

Redundancy of information can be used to do averaging or other types of filtering and improve the signal to noise ratio (S/N). However, not all measurements can be redundant. Consider a spectral phase function in two different cases:

a) All individual data points are used to represent the spectral phase *function*. The *final output* of phase measurement has as much *information* as all data points obtained in the measurement.

b) All data points are used to fit a line and the entire information is reduced to *one entity* (time delay) and some information is lost.

Real-time measurement of spectral phase cannot be done using a technique of Type (b) and there is no temporal or spectral redundancy. However, such a measurement can still be redundant in the sense of combining spatial data points (for example in imaging spectroscopy with a 2D camera).

4.1.5. Speed of Measurement

A real-time measurement scheme will provide considerable flexibility in alignment and compensation for different sources of error. Such a scheme can also characterize dynamics of time-varying structures and generate *phase spectrograms*. However, many phase measurements use some kind of scanning (moving a delay line, for instance) and cannot be done in real-time.

4.1.6. Wavelength of Operation

Using Ti-Sapphire lasers directly and working at sub-micron wavelengths has the benefit of having cheap detectors and cameras and cheap high resolution spectrometers. On the other hand, working at optical communication wavelengths is associated with the problem of very expensive Indium-based III-V detectors and cameras and low-resolution expensive spectrometers.

4.2. Proposed Method: Spectral Interferometry

4.2.1. Fundamentals of Spectral Interferometry

Interferometry maps optical phase shifts to intensities, and thereby makes indirect phase measurement possible. Interfering beams result in intensity fringes determined by the frequency of operation (ω) and the relative time delay between the two arms of the interferometer (τ). In pulse interferometry, ω assumes different values *simultaneously*, because of the wideband nature of the beam. τ is not changed during the measurement, either, and it is only changed for balancing the interferometer initially and optimizing the delay. These two features give rise to instantaneous measurements over the entire bandwidth of operation and real-time spectral phase measurements. A coherent wideband source is needed for spectral interferometry.

4.2.2. Measurement Setup and Alignment

The source is an optical parametric oscillator (Mira-OPO by APE Berlin GmbH) with a CTA (Cesium Titanyl Arsenate, $CsTiOAsO_4$) nonlinear crystal. The OPO is pumped by a Ti-Sapphire femtosecond laser (Mira 900 by Coherent Inc.) to generate two photons at

longer wavelengths. One photon from the Ti-Sapphire laser with a wavelength close to 800 nm is converted into two photons (*Signal* with the same polarization as the pump and *Idler* with the opposite polarization) at optical communication wavelengths. The wavelengths of the OPO outputs are controlled by changing the wavelength of the pump input. To be specific, our source is the *Idler* output of the OPO, which has a higher output power and can be tuned over a larger wavelength range close to 1550 nm. The OPO pulses have exactly the same repetition rate as the pump pulses (around 76 MHz) and almost equal or even a bit smaller pulse widths (around 100 femtoseconds). The average output power of the pump laser is around 1.5 W and that of the OPO can be up to 500 mW. By tuning the pump wavelength, it is possible to have femtosecond pulses at the output of the OPO in the wavelength range of 1490-1650 nm.

The pump laser is p-polarized (electric field is *parallel* to the optics table) and so, the *Idler* is s-polarized (electric field polarization is normal or *senkrecht*). The TE-like modes of PCWs have in-plane electric fields (p polarization). So, a half-wave plate is needed to change the linear polarization of the *Idler* from "s" to "p".

Specific optical elements for ultrafast experiments are usually offered at sub-micron wavelengths and not at optical communication wavelengths. A good choice for the half-wave plate is an *achromatic zero-order* half-wave plate with an almost flat retardation spectrum around the center wavelength.

There is a polarizing cube beam splitter in the OPO cavity to separate the *Signal* and *Idler*. Theoretically, this beam splitter, the optics table, the CTA nonlinear crystal, the half-wave plate, and the PCW must all be parallel to each other, so that "s" and "p" polarizations can be defined with respect to a unique system of coordinates. Using the

polarization optics in a rotation mount will provide a degree of freedom to somehow compensate for very small misalignments between the coordinate systems of the above mentioned components.

The beam from the source enters a Mach-Zehnder interferometer, where a delay line is used in the reference arm for balancing and tuning the interferometer and a waveguide (with input and output objective lenses) is put in the other arm. A microscope and an infrared (IR) camera are used to monitor the scattered IR light from the facet of the waveguide (as a feedback signal) during coupling optimization. The output of the waveguide is imaged onto a high-speed IR camera with a pixel pitch of 40 microns (SU320-1.7RT-V/RS170 by Sensors Unlimited Inc.). Using two apertures, the collimated beam from the reference arm and the spherical beam from the waveguide (imaged by an objective lens) are spatially-aligned. The collimated reference beam is then focused onto the slit of a monochromator/spectrograph (SpectraPro 150 by Acton Research Corp.), which is used as an imaging spectrometer. The same IR camera used for spatial profiling can be used for imaging spectroscopy; thereby reducing the cost considerably. The IR camera is then placed at the focal point of the output collimating mirror of the monochromator. The objective lens imaging the output of the waveguide is then moved by a small amount so that the waveguide output is imaged at the new position of the IR camera (where the beam from the reference arm has been imaged). Even without the spectrometer, the interference can be observed as sptial fringes. Spatial fringes indicate a relatively good temporal overlap, but also some spatial misalignment. They are only useful for alignment purposes and do not provide useful information for spectral interferometry.

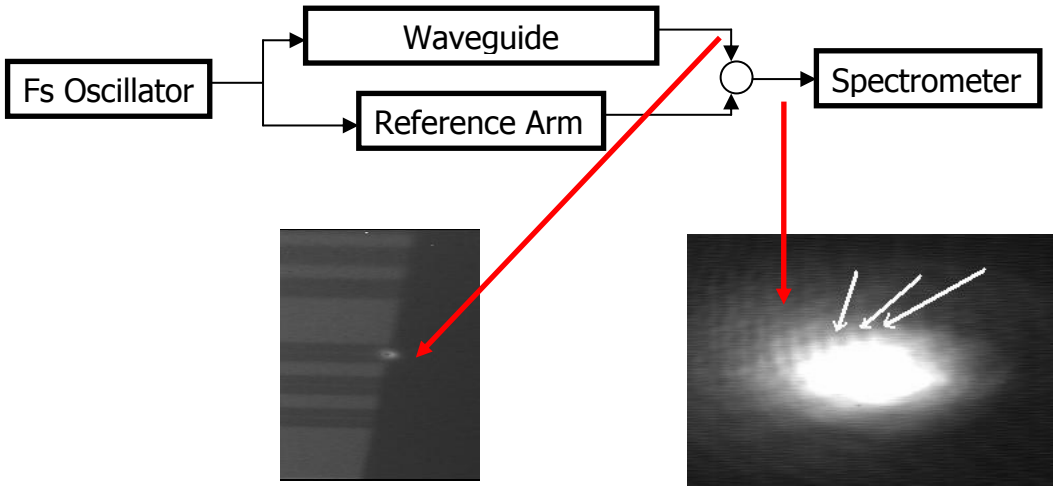

Figure 4.1. Block diagram of the setup (top); infrared images of the femtosecond pulse coming out of the waveguide (bottom left) and spatial fringes formed by interference of the beam from the waveguide with the reference beam (bottom right).

Horizontal alignment of the IR camera is done by centering the *reflection* off the grating on the camera. The grating is moved to a position corresponding to a wavelength of zero to reduce diffraction to simple reflection. Once the camera is positioned correctly, the grating is moved to a position corresponding to the center wavelength of the femtosecond pulse to see the spectrum and use the available bandwidth efficiently. If the slit has its minimum width and this horizontal alignment is done, one can use the theoretical formula to calibrate the spectrum. However, it is recommended that one use another spectrometer or the emission of reference lamps to calibrate the spectrometer. We use an optical spectrum analyzer (OSA 86142B by Agilent Technologies) for calibration. The OSA itself does not have enough sensitivity and also is not a real-time system, so it cannot be used as the spectrometer in our setup.

The grating of the monochromator has a density of 600 grooves/mm and the focal

length of the system is 150 mm. When the slit has its minimum width of 10 microns, both bandwidth per pixel and FWHM spectral resolution are smaller than 1 nm. Using a new IR camera with a pixel pitch of 25 microns and also using other gratings and focal lengths, we can improve the spectral resolution further. As a comparison, the spectral resolution of the NIR-512 spectrometer by Ocean Optics Inc. is around 3-5 nm.

The objective of the measurement is to see spectral fringes as shown in Figure 1. Once spectral fringes are observed, the delay line is moved by a small amount to change the relative phase shift and fringe spacing. The delay should be "small enough" and "large enough" to satisfy two antagonistic conditions imposed by the phase retrieval algorithm. Two such measurements on a reference and an unknown waveguide will determine the spectral phase of the unknown waveguide. Figure 4.2 shows spectral fringes observed by interference between the output of a ridge waveguide and the beam from the reference arm with a good position of the delay line.

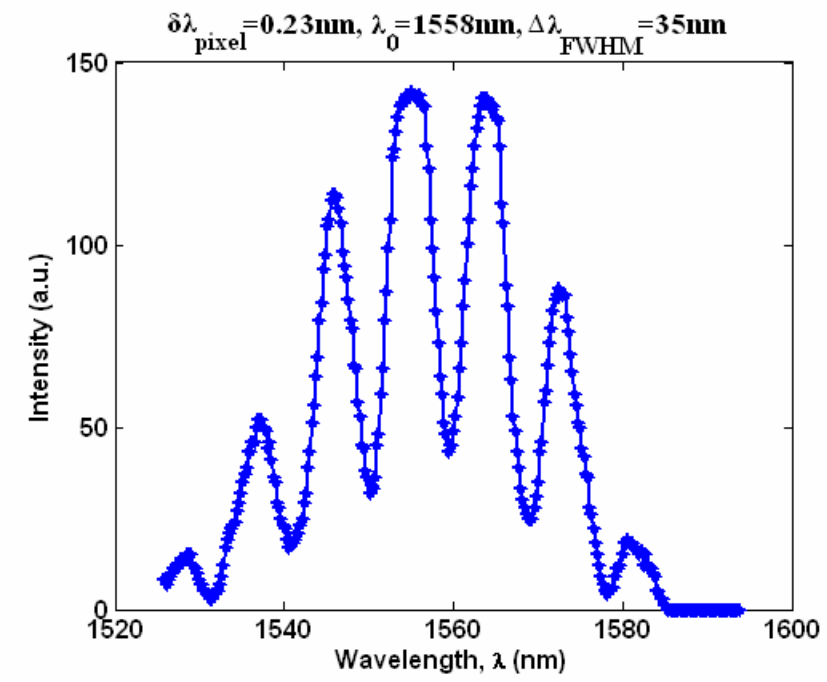

Figure 4.2. Measured spectral fringes

Note that there is no need to move the delay line during measurements. So, we use a manual micrometer to move the delay line. However, this manual micrometer is a differential micrometer with a resolution of 100 nm. This choice has made the setup very stable with the capability of fine tuning the delay between pulses.

4.2.3. From Spectral Fringes to Waveguide Dispersion

The spectral intensities of any arm of an interferometer can be measured by blocking the other arm. If no arm is blocked, one will measure the interference pattern. Knowing these three spectra and a simple interference equation, the cosine of the phase shift between the two arms as a function of frequency can be calculated. Polarization multiplexing can also be used to measure the sine of the phase shift simultaneously [52]. Knowing both sine and cosine of the phase shift, it can be uniquely determined. Unfortunately, this method is not applicable to our measurement, for a PCW has a completely different behavior for s-polarization.

Another common technique is Fourier Transform Spectral Interferometry (FTSI) [53,54]. The main idea is to take the inverse Fourier transform of spectral fringes; to select the right-most lobe (out of three lobes); and to take the Fourier transform.

4.2.3.1. Wavelength vs. Frequency

Experimental spectra are obtained as functions of equally-sampled wavelengths. Hence, such spectra represent power density per unit wavelength. Power density per unit frequency will not be obtained just by replacing wavelength with frequency. These two power densities represent two integrands that should be integrated over two different

variables to give the same value (total power). Changing the variable of integration will introduce an extra factor.

Also note that equidistant points in wavelength will not be equidistant in frequency and vice versa. The Fast Fourier Transform (FFT) algorithm is based on having equidistant samples of a function in time/frequency. Equidistant samples can be generated by interpolation between adjacent points.

4.2.3.2. Appropriate Delay

The position of the lobe we are interested in represents the delay between the two pulses. The delay should be large enough so that this lobe is distinguishable from the lobe centered at zero. For Gaussian pulses it means a delay at least five times the FWHM pulse width. The delay should also be small enough so that it fits into the available "time-width". Using the delay-line in the reference arm of the interferometer, one can easily achieve this requirement. Actually, we do these measurements for (at least two) different positions of the delay-line.

The abovementioned constraint on time delay is equivalent to having "reasonable" fringe spacing in frequency. Spectral fringe spacing should be small enough to see the variations and it should be large enough so that no aliasing occurs and fringe spacing remains larger than the resolution of the spectrometer. Such a value of delay is usually a few times the FWHM pulse width. In other words, good fringes do not correspond to overlapping pulses; rather they correspond to pulses with overlapping tails.

Also note that the distance between spectral fringes is the inverse of the delay between the pulses. So, an increase in temporal fringes results in a decrease in spectral

fringes. Both spectral and temporal fringes can be seen in FROG traces of a pulse. FROG traces can be used to balance an interferometer.

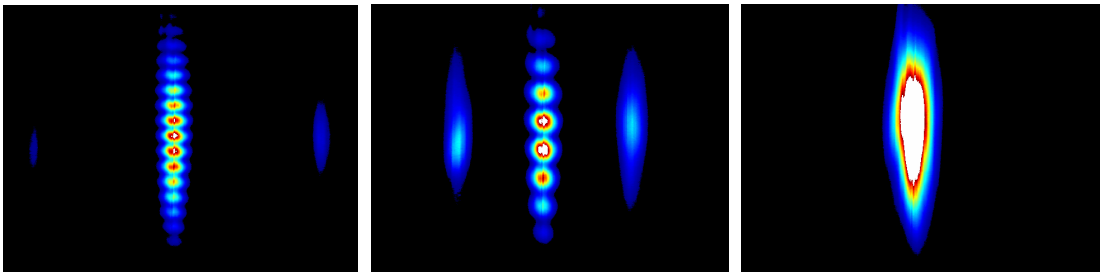

Figure 4.3. Measured FROG traces of the interferometer output (without a sample) for three positions of the delay line. As delay decreases and the two pulses overlap more and more, the distance between temporal (horizontal) fringes decreases, while the separation in frequency (vertical direction) increases. The leftmost figure corresponds to the largest delay; the middle one corresponds to a smaller delay; and the rightmost figure corresponds to a balanced interferometer (no delay).

4.2.3.3. Compensation for Unwanted Phase Shifts

The phase of the Fourier transform obtained in FTSI represents the spectral phase shift between the reference arm and the sample arm of the interferometer. In practice there are other elements such as objective lenses and neutral density filters in the interferometer, and the so-obtained phase cannot be attributed to the waveguide under study. Besides, the waveguide itself is connected to input and exit dielectric waveguides, tapers, and wider dielectric waveguides. Also, coupling into and out of the waveguide are also associated with some phase shifts.

One idea to eliminate these unwanted phase shifts is to fabricate two waveguides on the same substrate with similar tapers and input/exit dielectric waveguides. If alignment and cleavage are good, the difference between the results of phase shift measurements on two waveguides has only the signature of the two waveguides. If one of the waveguides is a simple *reference waveguide* with known dispersion, then the phase shift introduced by the unknown waveguide can be calculated.

Note that using just a dielectric waveguide as the reference is only acceptable when phase shifts introduced by coupling into and out of the waveguide under test are also accounted for. So, knowing just the dispersion of the reference waveguide will not be enough. An alternative *reference waveguide* is a shorter version of the waveguide under test (with other attached elements), which also takes these couplings into account.

The two waveguides must be characterized under similar conditions. We make sure that the beam focused on the sample will remain focused as the sample moves along the lateral direction all the way to the edges. Otherwise, the in-plane rotation of the sample will be eliminated to achieve this goal. We should also see the same scattering pattern in the vertical direction, as the sample moves. Otherwise, the tilt of the sample will be eliminated to achieve this goal. The accuracy of such an alignment can be improved by considering a large width for the sample, a small distance between the two waveguides, and a small pitch size for the IR camera monitoring the scattered beam.

The only thing that can somehow affect the measurements is improper cleavage of the sample. If the two waveguides are fabricated close to each other, this effect can be reduced. Also, these structures are usually duplicated during fabrication. So, if a pair of waveguides does not have similar cleavage, one can try other(s). Another solution is to use SEM images to find the profiles of cleavage and simulate the difference between phase shifts introduced by such a difference.

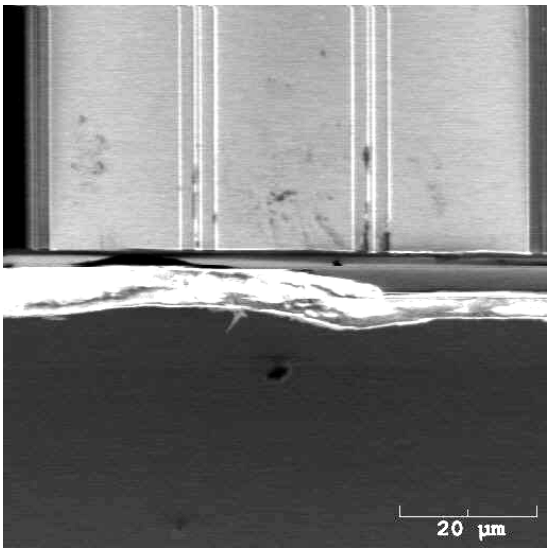

Figure 4.4. SEM image showing two parallel ridge waveguides oriented in the vertical direction. SEM imaging at this scale shows a relatively good cleavage at the top (Silicon) layer, which is the core of the waveguide. However, some irregularity in lower layers can be seen..

4.2.4. The Effect of Waveguide Length

The phase shift introduced by waveguide dispersion is proportional to the length of the waveguide under test (assuming single-mode operation and a dominant Floquet component). If the length is small, this phase shift will be small and may not be detected. On the other hand, if the waveguide is very long, the phase shift introduced by two consecutive measured frequencies may exceed 2π. It makes unwrapping the experimentally measured phase (limited to the interval $[-\pi, \pi]$) impossible, for β and $2\pi/L$ (L is the length of the waveguide) will result in the same value of phase. A long PCW will also have a large loss.

4.3. Simulation Results

A computer code has been developed to calibrate the measured spectra and calculate the spectral phase (and hence dispersion). A second code has been developed to generate arbitrary interfering pulses with different amplitudes, delays, and signal to noise ratio (S/N). The outputs of the latter have been used to verify and debug the former.

4.3.1. Unequal Amplitudes of Interfering Pulses

According to simulation results, if the amplitudes of two interfering pulses differ by a factor up to 50, the error in spectral phase is less than 1%. Such pulses will lead to "invisible" spectral fringes; however, the phase retrieval algorithm can still determine the spectral phase. In practice, the image recorded by a camera is quantized in amplitude and the dynamic range may not be enough. Besides, a beam with very small amplitude may have energy comparable to background noise. Hence, in practice, the pulses should have almost equal amplitudes.

4.3.2. Signal to Noise Ratio

With S/N=10 dB, the error in spectral phase will be smaller than 5% and with SN>20 dB, the error falls below 1%. In practice, quantization error of the frame grabber, finite dynamic range of the camera, and inefficient use of available dynamic range will increase the S/N required for a given minimum error.

4.3.3. Theory vs. Experiment

Figure 4.5 shows theoretical and experimental differences between the dispersion curves of a PCW and a reference ridge waveguide. The PCW has a lattice constant of a=400nm,

a second periodicity of *a'*=350nm, air hole radii of *r/a*=0.29, second radii of *r'/a*=0.17, a length of *L/a*=50, and a (silicon) slab thickness of *h*=220nm on top of a 3-micron thick underlying silica layer. Note that experimental results are in the range between -π and π and should be "unwrapped" to be comparable with theoretical results and match the dispersion diagrams. Phase unwrapping is done by addition of a discrete additive constant to match the experimental and theoretical values at one frequency, only. Figure 4.5 (drawn in the frequency range corresponding to high energy of the wideband source) shows a meaningful correspondence between theoretical and experimental results. Note that the measured phase is only valid at frequencies with relatively high amplitude of femtosecond pulses. The deviation from theory is small and is attributed to the above-mentioned different factors.

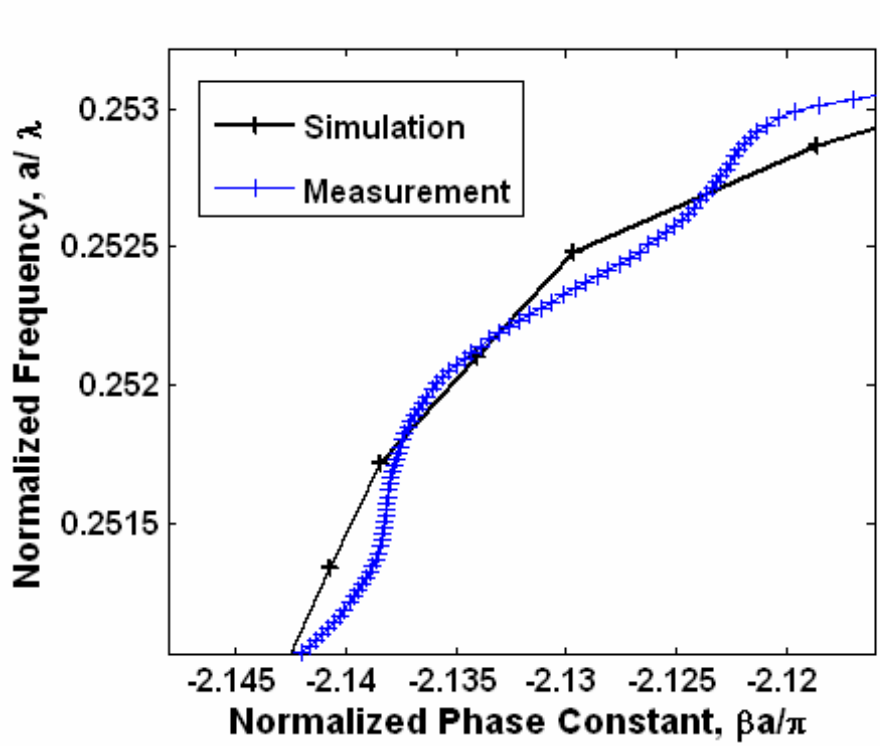

Figure 4.5. The difference between the dispersion of a PCW and that of a ridge waveguide

CHAPTER V

CONCLUSIONS AND FUTURE DIRECTIONS

5.1. Conclusions

In general, dispersion engineering in PCWs can be a complicated optimization problem with too many parameters. However, it has been shown that dispersion engineering in PCWs can be done by using only two parameters: the period and radius of air holes in the two rows close to the guiding region. Perturbing the size of these air holes can introduce an offset in the position of guided modes and this offset is different for even and odd modes. Perturbing the period of these air holes will shift the DBR peak frequency and modegap to other frequencies. By perturbing the period, it is possible to achieve linear dispersion and high transmission over large bandwidths (and even the entire PBG) in both straight and bent PCWs.

Perturbing the period of a PCW, will result in a multimode waveguide. Simultaneous perturbation of radius and period can resolve this issue and results in linear dispersion, high transmission, large guiding bandwidth, and single-mode operation below the light line. Experimental results also show very small loss coefficients in these waveguides, comparable to the loss coefficient of a ridge waveguide fabricated on the same substrate. A more rigorous and quantitative study of loss in biperiodic PCWs requires 3D simulations.

Conventional methods of dispersion calculation cannot be used to calculate the dispersion of such perturbed and nonperiodic waveguides. A method based on spatial Fourier transform of electromagnetic fields has been proposed to calculate dispersion in such waveguides. The flattening frequencies in the so-obtained dispersion diagrams agree very well with the edges of high-transmission windows in transmission diagrams. Diffracted orders and Bragg conditions in such waveguides have also been studied. The method used for dispersion calculation can be generalized to calculate complex modes of PCWs.

Complete characterization of PCWs requires the measurement of not only the transmission, but also the (spectral) phase or dispersion. A characterization technique based on spectral interferometry with femtosecond optical pulses at optical communication wavelengths has been successfully demonstrated. This technique is the first real-time measurement of dispersion in PCWs and can be used to study fast dynamics in structures such as sensors and MOEMS.

5.2. Proposed Research in the Area of PCW Optimization

a) Experimental demonstration of the trend in increasing (decreasing) the DBR peak frequency as the period decreases (increases).
b) Loss measurements with samples, which have better fabrication qualities
c) Experimental demonstration of the properties of structures, in which the second periods are close to each other, but one results in a *commensurate* and the other one in an *incommensurate* structure.
d) Completion of maps of Local Density of States (LDOS) as a function of

frequency, position, and perturbations in period and radius

e) 3D simulations of biperiodic PCWs

f) Experimental demonstration of biperiodic optical functionalities

5.3. Proposed Research in the Area of PCW Dispersion Measurement

a) Fabrication of different PCWs to have both gaps and guiding at OPO wavelengths of operation

b) Improving the performance of the setup by spatial and spectral filtering of the OPO output, using a high resolution frame grabber, better input coupling, integration of data acquisition and post-processing codes for real-time *observation* of spectral phase

c) Study of nonlinearity by changing the power launched into waveguides

d) Study of the effects of different distortions (chirp, pulse front tilt, ….) on the final retrieved phase

e) Using a commercial real-time spectrometer at optical communication wavelengths for easier spectral measurements and study of single-mode and multimode fiber coupling.

.

REFERENCES

[1] E. Yablonovitch, "Inhibited spontaneous emission in solid-state physics and electronics," *Physical Review Letters*, vol. 58, pp. 2059–2062, 1987.

[2] S. John, "Strong localization of photons in certain disordered dielectric superlattices," *Physical Review Letters,* vol. 58, pp. 2486–2489, 1987.

[3] S. John and J. Wang, "Quantum optics of localized light in a photonic band gap," *Physical Review B*, vol. 43, pp. 12772–12789, 1991.

[4] A. A. Asatryan, K. Busch, R. C. McPhedran, L. C. Botten, C. M. de Sterke, N. A. Nicorovici, "Two-dimensional Green's function and local density of states in photonic crystals consisting of a finite number of cylinders of infinite length," *Physical Review E,* vol. 63, pp. 046612/046615, 2001.

[5] M. Plihal and A. A. Maradudin, "Photonic band structure of two-dimensional systems: The triangular lattice," *Physical Review B*, vol. 44, pp. 8565–8571, 1991.

[6] S. Y. Lin, , E. Chow, V. Hietala, P. R. Villeneuve, and J.D. Joannopoulos, "Experimental demonstration of guiding and bending of electromagnetic waves in a photonic crystal," *Science*, vol. 282, pp. 274-276, 1998.

[7] A. Mekis, S. Fan, and J. D. Joannopoulos, "Bound states in photonic crystal waveguides and waveguide bends," *Physical Review B*, vol. 58, pp. 4809–4817, 1998.

[8] S. Y. Lin, V. M. Hietala, L. Wang, and E. D. Jones, "Highly dispersive photonic band-gap prism," *Optics Letters*, vol. 21, pp. 1771-1773, 1996.

[9] E. J. Reed, M. Soljačić, and J. D. Joannopoulos, "Color of shock waves in photonic crystals," *Physical Review Letters*, vol. 90, pp. 203904-203907, 2003.

[10] B. Momeni, J. Huang, M. Soltani, M. Askari, S. Mohammadi, M. Rakhshandehroo, and A. Adibi, "Compact wavelength demultiplexing using focusing negative index photonic crystal superprisms," *Optics Express*, vol. 14, pp. 2413-2422, 2006.

[11] J. D. Joannopoulos, R. D. Meade, and J. N. Winn, *Photonic Crystals: Molding the Flow of Light*, Princeton, NJ: Princeton Univ. Press, (1995).

[12] D. England, I. Fushman, and J. Vuckovic, "General recipe for designing photonic crystal cavities," *Optics Express*, vol. 13, pp. 5961-5975, 2005.

[13] A. Mekis, J. C. Chen, I. Kurland, S. Fan, P. R. Villeneuve, and J. D. Joannopoulos , "High transmission through sharp bends in photonic crystal waveguides," *Physical Review Letters*, vol. 77, pp. 3787-3790, 1996.

[14] B. Maes, P. Bienstman, R. Baets, "Switching in coupled nonlinear photonic-crystal resonators," *Journal of Optical Society of America B,* vol. 22, pp. 1778-1784, 2005.

[15] J. Yonekura, I. Mitsutaka, and T. Baba, "Analysis of finite 2-D photonic crystals of columns and lightwave devices using the scattering matrix method," *Journal of Lightwave Technology*, vol. 17, pp. 1500-1508, 1999.

[16] P. K. Kelly, J. G. Maloney, B. L. Shirley, R. L. Moore, "Photonic band structures of finite thickness: theory and experiment," *IEEE Antennas Propag. Soc. AP-S. Int. Symp.*, vol. 2, pp. 718-721, 1994.

[17] V.F. Rodriguez-Esquerre, M. Koshiba, H.E. Hernandez-Figueroa, "Finite-element analysis of photonic Crystal cavities: time and frequency domains," *Journal of Lightwave Technology*, vol. 23, pp. 1514-1521, 2005.

[18] Y. A. Vlasov, N. Moll, and S. J. McNab, "Mode mixing in asymmetric double-trench photonic crystal waveguides," *Journal of Applied Physics,* vol. 95, pp. 4538-4544, 2004.

[19] S. G. Johnson, S. Fan, P. R. Villeneuve, J. D. Joannopoulos, and L. A. Kolodziejski, "Guided modes in photonic crystal slabs," *Physical Review B*, vol. 60, pp. 5751-5758, 1999.

[20] T. Sondergaard, J. Arentoft, and M. Kristensen, "Theoretical analysis of finite-height semiconductor-on-insulator-based planar photonic crystal waveguides," *Journal of Lightwave Technology*, vol. 20, pp. 1619 –1626, 2002.

[21] T. Ochiai and K. Sakoda, "Dispersion relation and optical transmittance of a hexagonal photonic crystal slab," *Physical Review B*, vol. 63, pp. 125107-125113, 2001.

[22] K.S. Chiang, "Analysis of rectangular dielectric waveguides: effective-index method with built-in perturbation correction," *Electronics Letters*, vol. 28, pp. 388-390, 1992.

[23] A. Adibi, R. Lee, Y. Xu, A. Yariv, A. Scherer, "Design of photonic crystal optical waveguides with singlemode propagation in the photonic bandgap," *Electronics Letters*, vol. 16, pp. 1376-1378, 2000.

[24] S. McNab, N. Moll, and Y. Vlasov, "Ultra-low loss photonic integrated circuit with

membrane-type photonic crystal waveguides," *Optics Express*, vol. 11, pp: 2927-2939, 2003.

[25] C. G. Bostan, R. M. de Ridder, V. J. Gadgil, H. Kelderman , L. Kuipers, and A. Driessen, "Design and fabrication of line-defect waveguides in hexagon-type SOI photonic crystal slabs," *Proceedings of the SPIE,* vol. 5450, pp. 323-332, 2004.

[26] A. Jafarpour, A. Adibi, Y. Xu, and R. K. Lee, "Mode dispersion in biperiodic photonic crystal waveguides", *Physical Review B*, vol. 68, pp. 233102- 233105, 2003.

[27] S. G. Johnson, P. R. Villeneuve, S. Fan, and J. D. Joannopoulos , "Linear waveguides in photonic-crystal slabs," *Physical Review B,* vol. 62, pp. 8212–8222, 2000.

[28] Y. A. Vlasov, N. Moll, and S. J. McNab, "Mode mixing in asymmetric double-trench photonic crystal waveguides," *Journal of Applied Physics,* vol. 95, pp. 4538-4544, 2004.

[29] T. Baba, A. Motegi, T. Iwai, N. Fukaya, Y. Watanabe, and A. Sakai, "Light propagation characteristics of straight single-line-defectwaveguides in photonic crystal slabs fabricated into asilicon-on-insulator substrate," *IEEE Journal of Quantum Electronics*, vol. 38, pp. 743-752, 2002.

[30] N. Moll and G. L. Bona, "Comparison of three-dimensional photonic crystal slab waveguides with two-dimensional photonic crystal waveguides: Efficient butt coupling into these photonic crystal waveguides," *Journal of Applied Physics*, vol. 93, pp. 4986-4991, 2003.

[31] M. Qiu, K. Azizi, A. Karlsson, M. Swillo, and B. Jaskorzynska, " Numerical studies of mode gaps and coupling efficiency for line-defect waveguides in two-dimensional photonic crystals," *Physical Review B*, vol. 64, pp. 155113-155117, 2001.

[32] T. Baba, D. Mori, K. Inoshita, and Y. Kuroki, "Light localizations in photonic crystal line defect waveguides," *IEEE Selected Topics in Quantum Electron*ics, vol 10, pp. 484-491, 2004.

[33] M. Badieirostami, B. Momeni, M. Soltani, A. Adibi, Y. Xu, and R. Lee, "Investigation of physical mechanisms in coupling photonic crystal waveguiding structures," *Optics Express*, vol. 12, pp. 4781-4789, 2004

[34] T. Søndergaard and K. H. Dridi, "Energy flow in photonic crystal waveguides," *Physical Review B*, vol. 61, pp. 15688–15696, 2000.

[35] M. Loncar, J. Vuckovic, and A. Scherer, "Methods for controlling positions of guided modes of photonic-crystal waveguides," *Journal of Optical Society of America* B, vol. 18, pp. 1362-1368.

[36] A. Adibi, R. Lee, Y. Xu, A. Yariv, A. Scherer, “Design of photonic crystal optical waveguides with singlemode propagation in the photonic bandgap,” *Electronics Letters*, vol. 16, pp. 1376-1378, 2000.

[37] K. Yamada, M. Notomi, A. Shinya, C. Takahashi, J. Takahashi, and H. Morita, “Single-mode lightwave transmission in SOI-type photonic-crystal line-defect waveguides with phase-shifted holes,” *Electronics Letters*, vol. 38, pp. 74-75, 2002.

[38] W. T. Lau and S. Fan, “Creating large bandwidth line defects by embedding dielectric waveguides into photonic crystal slabs,” *Applied Physics Letters*, vol. 81, pp. 3915-3917, 2002.

[39] T. Søndergaard and A. Lavrinenko, “Large-bandwidth planar photonic crystal waveguides,” *Optics Communications*, vol. 203, pp. 263-270, 2002

[40] J. P. Berenger, "A perfectly matched layer for the absorption of electromagnetic waves," *Journal of Computational Physics*, vol. 114, pp. 185-200 ,1994.

[41] A. Jafarpour, C. M. Reinke, A. Adibi, Y. Xu, and R. K. Lee, “A New Method for the calculation of the Dispersion of Non-Periodic Photonic Crystal Waveguides,” *Journal of Quantum Electronics*, vol. 40, pp. 1060-1067, 2004.

[42] A. Chutinan, M. Okano and S. Noda, "Wider bandwidth with high transmission through waveguide bends in two-dimensional photonic crystal slabs," *Applied Physics Letters*, vol. 80, pp. 1698-1700, 2002.

[43] A. Jafarpour, A. Adibi, Y. Xu, and R. K. Lee, “Integrated Optical Functionalities Featuring Bi-Periodic Photonic Crystals,” *Conference on Lasers and Electro Optics (CLEO)*, Baltimore, Maryland, USA, 2005.

[44] T. Tamir, Ed., *Guided Wave Optoelectronics*, Springer Verlag, New York, 1988

[45] D. Michaelis, U. Peschel, C. Wächter, and A. Bräuer, “Reciprocity theorem and perturbation theory for photonic crystal waveguides,” *Physical Review E*, vol. 68, pp. 065601-065604, 2003.

[46] S. G. Johnson, P. Bienstman1, M. A. Skorobogatiy, M. Ibanescu, E. Lidorikis, and J. D. Joannopoulos, “Adiabatic theorem and continuous coupled-mode theory for efficient taper transitions in photonic crystals,” *Physical review E*, vol. 66, pp. 066608-066622, 2002.

[47] A. Jafarpour, E. Chow, C. M. Reinke, J. D. Huang, A. Adibi, A. Grot, L. W. Mirkarimi, G. Girolami, R. K. Lee, and Y. Xu, “Large-bandwidth ultra-low-loss guiding in biperiodic photonic crystal waveguides,” *Applied Physics B*, vol. 79, pp. 409-414,

2004.

[48] M. C. Gupta and S. T. Peng, “Diffraction of a light beam by doubly periodic structures,” *Optics Letters*, vol. 16, pp. 1301-1303, 1991.

[49] B. T. Rosner, G. J. Schneider, and G. H. Watson, “Interferometric investigation of photonic band-structure effects in pure and doped colloidal crystals,” *Journal of Optical Society of America B*, vol. 15, pp. 2654-2659, 1998.

[50] M. C. Netti, C. E. Finlayson, J. J. Baumberg, M. D. B. Charlton, M. E. Zoorob, J. S. Wilkinson, and G. J. Parker, “Separation of photonic crystal waveguides modes using femtosecond time-of-flight,” *Applied Physics Letters*, vol. 81, pp. 3927–3929, 2002.

[51] M.L.M. Balistreri, H. Gersen, J.P. Korterik, L. Kuipers, and N.F. van Hulst, “Tracking femtosecond laser pulses in space and time,” *Science*, 294, 1080-1082 (2001).

[52] L. Lepetit, G. Cheriaux, M. Joffre, “Linear techniques of phase measurement by femtosecond spectral interferometry for applications in spectroscopy,” *Journal of Optical Society of America B*, vol. 12, pp. 2467-2474, 1995.

[53] D. N. Fittinghoff, J. L. Bowie, J. N. Sweetser, R. T. Jennings, M. A. Krumbugel, K. W. DeLong, R. Trebino, and I. A. Walmsley, “Measurement of the intensity and phase of ultraweak, ultrashort laser pulses,” *Optics Letters*, vol. 21, pp. 884-886, 1996; “Erratum,” vol. 21, pp. 1313-1315, 1996.

[54] C. Dorrer, N. Belabas, J.P. Likforman, and M. Joffre, “Spectral resolution and sampling issues in Fourier-transform spectral interferometry,” *Journal of Optical Society of America B*, vol. 17, pp. 1795-1802, 2000.